9-30-2016

Localization and Investigation of Secondary Metabolite Producing Styela clava-Associated Streptomyces Bacteria

James deMayo
University of Connecticut - Storrs, james.demayo@uconn.edu

Localization and Investigation of Secondary Metabolite Producing *Styela clava*-Associated *Streptomyces* Bacteria

James A. deMayo

B.S. University of California, Santa Barbara, 2013

A Thesis

Submitted in Partial Fulfillment of the

Requirements for the Degree of

Master of Science

At the

University of Connecticut

2016

APPROVAL PAGE

Master of Science Thesis

Localization and Investigation of Secondary Metabolite Producing *Styela clava*-Associated *Streptomyces* Bacteria

Presented by James Abraham deMayo

B.S.

Major Advisor_____

Marcy J. Balunas

Associate Advisor_____

M. Kyle Hadden

Associate Advisor_____

Andrew Wiemer

Associate Advisor_____

Jonathan L. Klassen

Associate Advisor_____

Adam Zweifach

Associate Advisor_____

Dennis L. Wright

University of Connecticut

2016

Acknowledgments

I would first like to thank my advisor, Dr. Marcy Balunas, for guiding me through my first educational experience at the graduate level and for supporting me through my studies. I would like to thank my thesis committee, Drs. Jonathan Klassen, Adam Zweifach, Dennis Wright, M. Kyle Hadden, Andrew Wiemer, and Amy Anderson for valuable mentoring, assistance, and advice in completing the research portions of my degree. I owe a great deal of thanks to the members of the Wright and Anderson labs who have helped guide me during experiments, and to the members of the Klassen lab who provided materials for completion of bacterial culturing. A special thanks goes to Ziyan Zhao and the Zweifach lab who co-authored my first publication and provided the CTL biodata that helped us isolate our natural product. Thank you to Dr. Vitaliy Gorbatyuk for endless help with collecting NMR data and to Dr. You-Jun Fu for collection of the high resolution mass spectra. Thank you to Drs. Carolyn Teschke and Tina Motwani for help with performing of the circular dichroism experiments. I also thank Dr. Emily Mevers for help with collection of the polarimetry data. Dr. Kendra Maas and the UConn MARS facility also deserve a big thank you for their endless help in genome sequencing. I also thank members of the UConn DNA biotech facility for their help in Sanger sequencing of PCR products. Thank you also to Jeff Amberg and the team at Retrogen, Inc. for their help in sequencing our DNA. I would also like to thank the members of the graduate school and Multicultural Scholars Program, especially Charmane Thurmand, for providing financial support during my time as a Master's student.

I appreciate the help of the members of my lab, Annie Sung, Jillian Garcia, Danielle L'Heureux, Matthew Lin, Heather Winter, Andrew Maxwell, and Brendan Stewart. Special thanks to Ann-Chee Cheng who originally isolated the bacterium that we were able to culture and extract. The biggest thanks goes to Samantha Gromek for guiding me through my first two years as a

graduate student and helping teach me the proper techniques I needed to complete this research. Thank you also to Supriya Singh and the Rasmussen lab for assistance in measuring DNA concentrations and for use of the Gel Doc camera to capture my results. I owe a big debt a gratitude to Ashley West, who began the work that eventually transformed into my Master's thesis. She is not only a hardworking, brilliant student, but a fierce and most valuable friend.

I would finally like to thank members of my friends and family who helped me get accustomed to life in Connecticut. Thanks to Jen and Jim for listening and helping me adjust to graduate school. Thanks to my grandmothers, Sarina Sabin and Molly deMayo who provided the inspiration and strength to keep moving forward. Many thanks are given to Alex Estrada, Kathryn Fernberg, Liz Tencza, and Julie Silverman for their fantastic friendships. Thank you to Katie Rollins for helping me in my journey to the east coast. Finally, I would like to thank my parents, Celia and Bob deMayo, who have never wavered in their support of my quest for education. And thank you to my brother, Benny deMayo, who has always offered a stable ear to listen when I need it and being the best friend a brother could ask for.

Contents

List of Figures

List of Tables

Abstract

Natural products and natural product derivatives comprise some of the most successful drugs to date. Many natural products derive from the secondary metabolite profiles of high GC content actinomycete bacteria of the genus *Streptomyces*, which are sometimes associated with eukaryotic hosts. Identification of biosynthetic gene sequences for natural product secondary metabolites in *Streptomyces* can assist in isolation of the identified natural product. Moreover, the biosynthetic pathways of drug-like secondary metabolites derived from *Streptomyces* bacteria often provide insight into the available metabolites that can be produced. As a result, identification of bacteria capable of producing antibacterial products, including *Streptomyces*, can often lead to identification of biologically relevant secondary metabolites.

It has been hypothesized that symbiotic relationships between invertebrate hosts and bacteria have evolved to protect host organisms from pathogenic invasion. Many invertebrates contain only an innate immune system incapable of adaptation, suggesting one hypothesis that this primitive immunity may be supplemented through the presence of symbiotic bacteria. To identify immune system augmenting methods, recent research has identified new techniques that investigate adaptive immune system enhancement through protein kinase C (PKC) activation and calcium channel influx in addition to suppression.

The research described here investigated a novel strain of antibiotic-producing *Streptomyces*, isolated from the invasive tunicate *Styela clava* collected from the University of Connecticut at Avery Point (Groton, CT). During the investigation of the secondary metabolite production, tumor promoting and PKC activating metabolite teleocidin A-1 was identified via a novel assay screen. The assay screen was designed to investigate small molecules that can enhance lytic granule exocytosis from cytotoxic T-lymphocytes either by stimulating calcium influx or

activation of PKC. Identification of teleocidin A-1 inspired further investigation as to whether the bacterial secondary metabolite is developed to influence specific pathways of the host tunicate immune system. This hypothesis was investigated through attempts to localize the bacteria producing teleocidin A-1 to specific areas within the tunicate, including the gut and outer tunic. It was hypothesized that bacterial localization in or around various organs would lead to influence by secondary metabolites produced by bacteria, including teleocidin A-1. Thus, localization of bacteria by the host may indicate an influence by secondary metabolites on various organs and organ systems. Whole genome sequencing was employed to identify biosynthetic gene clusters that might play a role in antibiotic natural product biosynthesis as well as biosynthesis of teleocidin. After sequencing the bacterial genome, DNA samples isolated from various tunicate tissues were examined for bacterial DNA involved in the biosynthesis of teleocidin and for the presence of other antibiotic-producing *Streptomyces* bacteria. Results from localization experiments indicate that bacteria associated with antibiotic and natural product production are localized within the tunicate body, but not within the outer tunic membrane.

Keywords: teleocidin, *Streptomyces*, *Styela clava*, bacteria, tunicate, secondary metabolites, natural products

I. Introduction

Marine invertebrates and their associated microorganisms can produce ecologically and physiologically relevant bioactive secondary metabolites (Kobayashi and Ishibashi, 1993). In particular, organisms from the phylum Urochordata are responsible for the production of novel metabolites such as cephalostatin, derived from the hemichordate marine tube worm, *Cephalodiscus gilchristi,* mandelalides isolated from the marine ascidian *Lissoclinum* sp., and methicillin-resistant *Staphylococcus aureus* (MRSA) pyruvate kinase-inhibiting bisindole alkaloids derived from the marine sponge, *Topsentia pachastrelloides* (Davies-Coleman and Veale, 2015). Natural products isolated from tunicates have a history of success as anti-cancer drugs or drug leads including didemnin B, plitidepsin, and ecteinascidin 743 (Figure 1) (Rinehart, 2000). Didemnin B was isolated from tunicates located in the Caribbean, while ptlitidepsin and ecteinascidin 743 were isolated from the tunicates *Aplidium albicans* and *Ecteinascidia turbinata*, respectively. Late phase clinical trial research for the treatment of leukemia, melanoma, ovarian cancer, breast, prostrate, and gastric tumors as well as non-small cell lung tumors was examined with didemnin B and plitidepsin (Sakai, et al., 1996). Similarly, ecteinascidin 743 has been approved for treatment of soft-tissue sarcoma and is in clinical trials for the treatment of breast, melanoma, non-small cell lung, and ovarian cancers (Sakai, et al., 1996).

The previously mentioned drug candidates represent a portion of the large number of natural products isolated directly from tunicates. Many of the natural products isolated from tunicates contain peptidic, polyketide, alkaloid, and terpenoid structural motifs, which resemble structural compounds derived from symbiotic and associated bacteria (Schmidt and Donia, 2010). Indeed, it has been suggested that the true source for ascidian secondary metabolite natural products derives from bacteria (Ireland and Scheuer, 1980). In addition to tunicates there

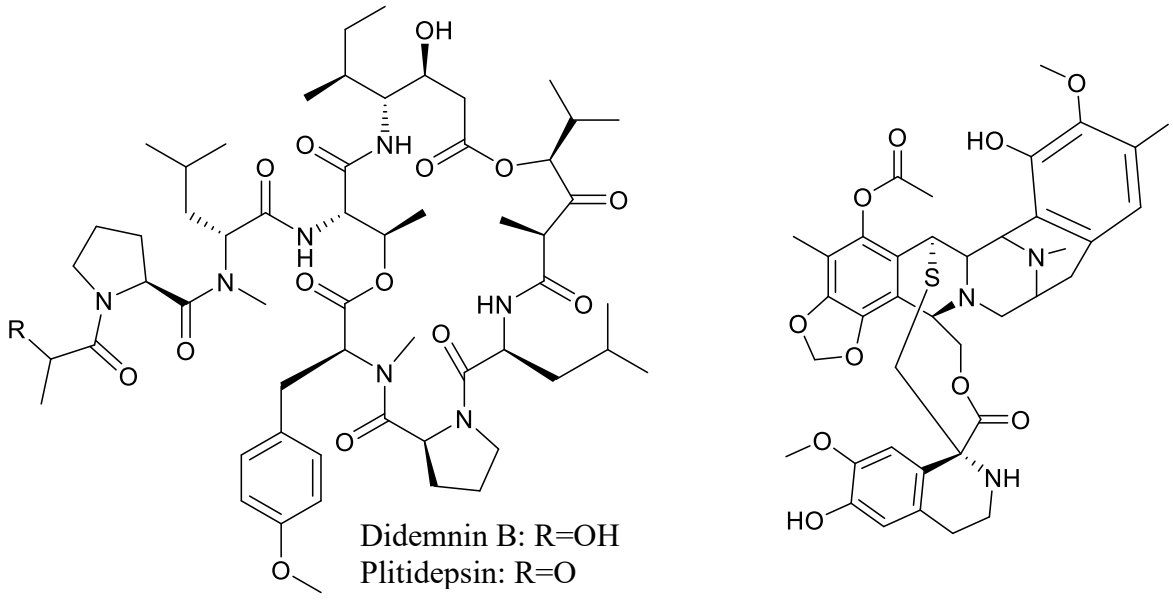

Figure 1. Drug candidates derived from tunicates. Structures of didemnin B and plitidepsin (left), and ecteinascidin 743 (right) all isolated from tunicates (Rinehart, 2000). All three have entered late stage clinical trials for treatments of select cancers. Ecteinascidin 743 has been approved for the treatment of soft-tissue sarcomas, while the didemnins are still investigated in clinical trials.

have been several biologically relevant natural products associated with bacteria that are isolated from other marine invertebrates (Lopanik, 2014). In fact, bacteria associated with marine invertebrates have been implicated in the production of some of the more potent chemical defense mechanisms including the production of 2,3-indolinedione (isatin) (Gil-Turnes, et. al., 1989). Isatin has been utilized as a antifungal metabolite and identified in the chemical defense of the estuarine shrimp *Palaemon macrodactylus* against pathogenic fungi, namely *Lagenidium callinectes.* Octalactin A was also isolated from marine *Streptomyces* and exhibited strong cytotoxic activity towards human colon cancer (Tapiolas, et al., 1991). Other cytotoxic compounds isolated from marine bacteria include alteramide A, isolated from a bacterium of the genus *Alteromonas*, derived from the Japanese sponge *Halichondria okadai* (Shigemori, et al., 1992).

While several successful chemical defense secondary metabolites have been identified from marine host-associated bacteria, a review by Lopanik (2014) highlighted that identification of chemical defense symbiosis is accompanied by a number of challenges. For example, they suggest that in order to illustrate definitive chemical defense symbioses, sophisticated techniques for structure elucidation and symbiont localization are necessary such as chromatography and mass spectrometry. In addition, Lopanik (2014) indicates that it is necessary to demonstrate reproductive and defense system failure as a result of removing the symbiotic bacteria in order to reveal the bacterial role in preserving the health and survival of the host. Curing the host from its natural product-producing symbiont without removal of other associated microbes may be difficult if the relationship between the organisms is obligate. Moreover, if the bacteria responsible for producing the biological natural product is unculturable, reintroduction into the host-symbiont system may be unattainable. In addition, Moran, et al. (2008) suggested that the removal of a microbial symbiont followed by reintroduction into the environment may lead to genomic deterioration. The

review by Lopanik (2014) discussed that bioactive natural products produced by symbiotic microorganisms contribute to the chemical defense mechanisms used by invertebrate hosts despite the challenges associated with demonstrating a natural product defensive symbiosis. Finally, removal of the symbionts responsible for the chemical defenses can often lead to decreased growth rates and lowered viability amongst host invertebrates (Lopanik, 2014).

Protection and immunity for select marine invertebrates has evolved to include symbiotic microorganisms and their natural products. Marine invertebrates that possess an innate immune system have evolved a variety of complex mechanisms to compensate for their lack of a true adaptive immune system (Rowley and Powell, 2007). Examples of these mechanisms include utilizing symbiotic bacteria as external defense against disease and pathogens (Kobayashi and Ishibashi, 1993). While tunicates lack an adaptive system that is capable of acquiring immunity, tunicates do possess an innate immune system which includes a highly polymorphic allorecognition response system used to recognize individuals of the same species and maintain species homogeneity (De Tomaso, 2009). Previous research by De Tomaso (2009) asserts that the allorecognition responses to external stimuli serve as the evolutionary origin for intracellular polymorphic recognition strategies present in vertebrate adaptive immune systems. The colonial tunicate *Botryllus schlosseri* has been extensively studied for its allorecognition response (Taketa, et al., 2015). This colonial tunicate is characterized by a group of individual, asexually derived, genetically identical zooids that are connected by a central vascular network (Figure 2) (Manni, et al., 2007). While previous research has examined the availability of bacteria within colonial tunicates (Dishaw, et al., 2014), less research has been performed examining the presence of associated bacteria amongst solitary tunicates. Zooids that comprise colonial tunicates have adopted sophisticated methods of allorecognition to recognize colony members have been

extensively researched for colonial tunicates (Dishaw, et al., 2014). The edges of the colony contain the allorecognition site characterized by small protrusions known as ampullae (De Tomaso, 2009). Previous research performed by Scofield, et al. (1982) identified that as colonies grow and come into contact with one another, the need for self-recognition systems becomes necessary. De Tomaso (2009) described that functional allorecognition responses will recognize genetically identical individuals and merge vasculature. Moreover, non-functional responses will reject the nearby ampullae and mount an inflammatory immune response. De Tomaso (2009) also demonstrated that allorecognition for tunicate colonies of *Botryllus schlosseri* is controlled by the *fusion/histocompatibility* (*fuhc*) gene locus. Individuals sharing one or two of the same alleles on this locus will merge together, while those with none will be rejected. Tunicates with incompatible alleles at the *fuhc* locus will undergo an inflammatory response resulting in a melanin scar at the site of interaction, which parallels natural killer cell mechanisms that destroy target cells if no self-markers are present (Long, et al., 2013). In solitary tunicates, it has been proposed that similar histocompatibility reactivity governs the ability to recognize individuals with similar alleles despite differences in mating potential (Fuke and Numakunai, 1982).

Several characteristics of the tunicate immune system are phylogenetically related to homologous aspects of mammalian immune systems. In particular, research by Vizzini, et al. (2015) has suggested that regulation of inflammation via cytokine IL-17 in solitary tunicate species shares a close relationship to mammalian cytokines, and thus likely shares a common chordate immune system ancestor. Specifically, IL-17 cytokine production is implied in the clearance of extracellular bacteria. Given that symbiotic bacteria may be providing chemical defense for their invertebrate hosts, ability to distinguish helpful versus harmful microorganisms becomes significant in the defense system for the host tunicate. Furthermore, ability to modulate immune

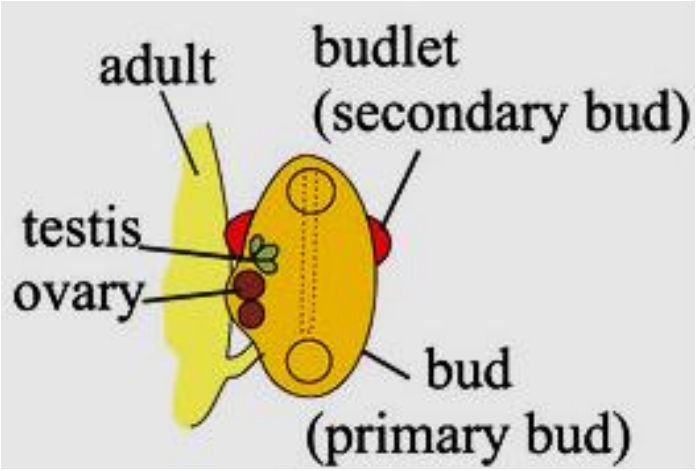

Figure 2. Colonial tunicate oozooids. Asexual reproduction of *Botryllus schlosseri* allows for identical zooid growth from the adult tunicate individual. All buds are connected by a central vascular network (Manni, et al., 2007). Recognition of unidentical tissue not produced by asexual budding allows for defense against pathogenic invasion. Figure modified from Gasparini, et. al. (2014).

system function becomes even more significant considering that associated bacteria may be responsible for secondary metabolites that influence immune system function and can contribute to defense against pathogen invasion. Bacteria that are responsible for natural product production involved in chemical defense of the host organism, thus, may not be cleared via immune system processes and may be involved in the production of immune system modifying secondary metabolites such as griseusrazin A which is derived from *Streptomyces griseus* (Lee, et al., 2016). Moreover, Erwin, et al. (2013) demonstrated that invasive tunicate species have a high degree of bacterial diversity and that the presence of a diverse population of associated bacteria allows for effective acclimation upon colonization for solitary invasive species.

The high degree of diversity associated with tunicate associated bacteria results in a diverse set of biologically active natural products. In particular, marine associated actinobacteria have been implicated in the production of potent toxic natural product alkaloids that can result in human disease and pose a toxicological threat to native wildlife. For example, teleocidin A-1 (**1**) (Figure 3) is an indolactam-V based secondary metabolite originally isolated from a marine *Streptomyces* bacteria known for toxicity to Japanese killifish (Takashima and Sakai, 1960). Research by Wang, et al. (1999) has shown **1** to be a potent tumor promoter and activator of protein kinase C (PKC). Specifically, Wang, et al. (1999) demonstrated that the indolactam-V scaffold from which **1** is based has been demonstrated to bind the C1B domain of PKC during activation similar to phorbol myrsitate acetate (PMA). In addition, stimulation of killer T-cells as part of immune responses occurs by two mechanisms: calcium influx and activation of PKC and ERK pathways (Pores-Fernando and Zweifach, 2009). Two specific conformations of the indolactam-V scaffold have been identified for the binding events within the C1B binding domain of PKC (Wang, et al., 1999). These conformations are known as cis-twist and trans-sofa. While both conformations exist in

solution, the cis-twist conformation has been demonstrated as the conformation responsible for PKC activation (Wang, et al., 1999). Enantiomeric derivatives of **1** have been demonstrated to have over one hundred times weaker binding affinity than **1**, and structural derivatives of **1** have been identified as tumor promoters, though with less activity as compared to **1** as a result of stereospecificity during binding (Jiang, et al., 2014).

In 1979, **1** was isolated again from a marine cyanobacterium *Moorea producens* (formerly *Lyngbya majuscula*) and named lyngbyatoxin A (Cardellina II, et. al. 1979). The biosynthesis scheme for lyngbyatoxin A was first characterized from the marine cyanobacteria *Moorea producens* prior to the identification of teleocidin biosynthetic pathways (Figure 4) (Edwards and Gerwick, 2004). The proposed biosynthesis for lyngbyatoxin A incudes a modified NRPS/PKS pathway with four relevant genes that code for one dimodular nonribosomal peptide synthetase, a unique prenyltransferase, an MbtH-Cytochrome P-450 monooxygenase, and one reductase/oxidase enzyme . It was suggested that the involvement of the reductase/oxidase enzyme was used in the conversion from lyngbyatoxin A to derivatives lyngbyatoxin B and C (Figure 4) (Edwards and Gerwick, 2004). Because structural and enantiomeric derivatives were shown to be less potent PKC activators and tumor promoters than **1**, it has been suggested that the biosynthesis of teleocidin and lyngbyatoxin derivatives may be used to regulate the relative toxicity of the local environment during secretion (Jiang, et al., 2014). More recently, Awakawa et al. (2014) identified gene homologs in teleocidin producing *Streptomyces* strains with the same catalytic domain structures as the lyngbyatoxin biosynthesis scheme published by Edwards and Gerwick (2004). In essence, homologs for the protein catalytic domains involved in the biosynthesis of lyngbyatoxin A were identified in the genome of teleocidin producing *Streptomyces* and designated as the teleocidin-producing biosynthetic gene cluster. The teleocidin-producing biosynthetic gene cluster

(*tle*) encodes for the same nonribosomal peptide synthetase (*tleA*), P-450 monooxygenase (*tleB*), and aromatic prenyltransferase (*tleC*) as previously identified for lyngbyatoxin. In addition, in certain *Streptomyces*, a fourth methyltransferase gene (*tleD*) identified downstream of the *tle* biosynthetic gene cluster has been characterized in the conversion of **1** to teleocidin B (**2**) (Figure 3) (Awakawa, et al., 2014).

In this research, immune system responses were used to investigate the potential relationship roles between tunicate associated *Streptomyces* and *Styela clava*. It is hypothesized in this research that based on previous research concerning the roles of host-associated bacteria with marine tunicates, the bacterium involved in the production of **1** may be involved in protection or modification of tunicate immune system function via incorporation of biologically relevant secondary metabolites as chemical defense to supplement the lack of a true adaptive immune system. As a result, the biosynthetic capacity of the bacteria for production of **1** and for its production of other biologically relevant secondary metabolites was investigated.

Specific Aim 1: To analyze the role that the tunicate-associated bacterially-derived natural product plays in its interactions with associated invertebrates, the first aim involves a thorough analysis of immunomodulatory biological activity of bacterial extracts. To accomplish this, a novel cytotoxic T-lymphocyte (CTL) bioassay was employed to examine the amount of enhanced stimulation and/or suppression of CTL lytic granule exocytosis. An indole alkaloid natural product isolated from tunicate-associated *Streptomyces* was identified, isolated, and characterized in order to identify a potential mechanism for this natural product associated with marine derived bacteria acts through.

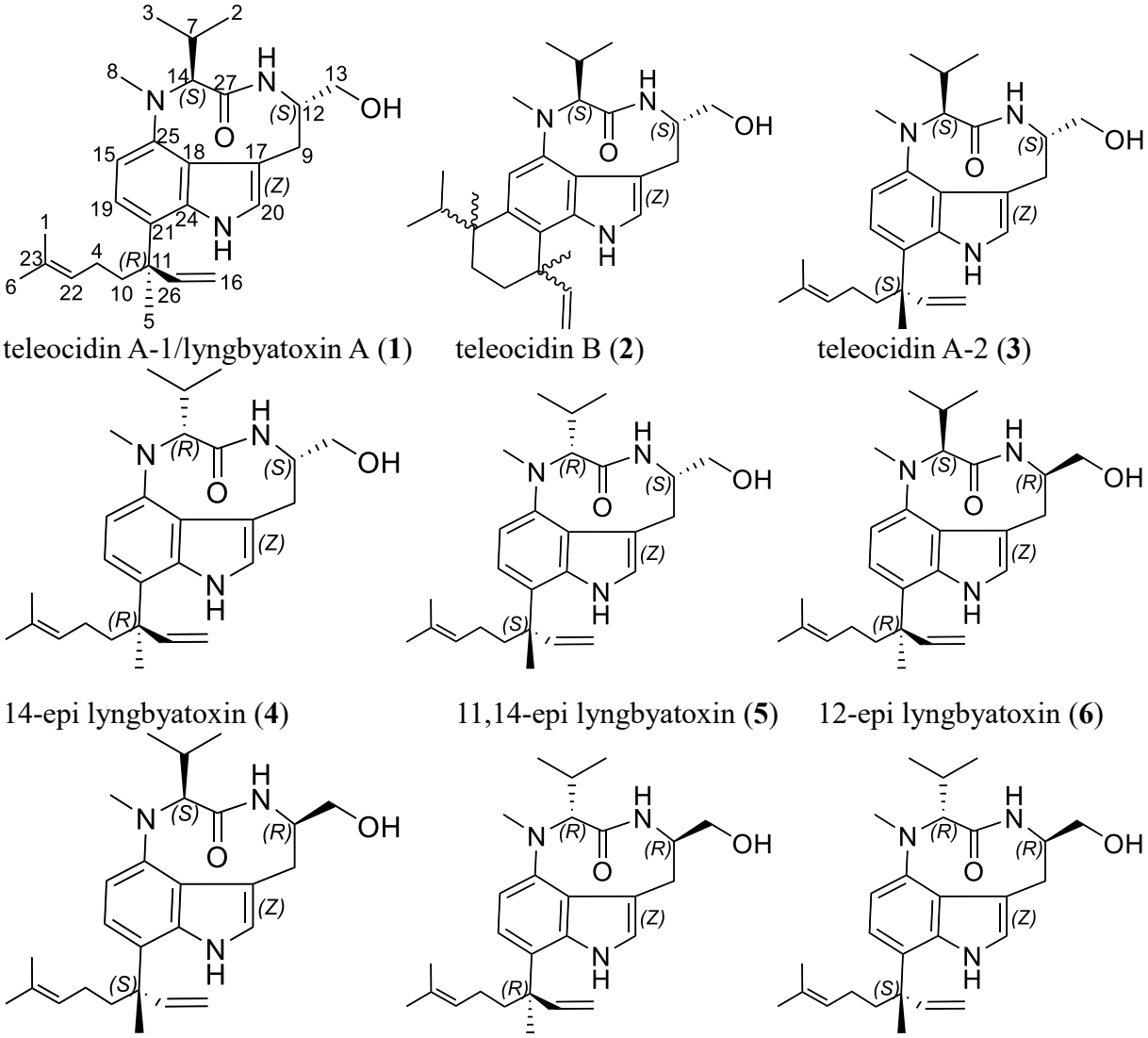

Figure 3. Teleocidin derivative structures. Structures and assignment of carbon atoms for **1** (teleocidin A-1; top left) are included with theoretically possible enantiomers including structural derivative **2** (teleocidin B; top middle) and naturally occurring **3** (teleocidin A-2; top right) and **4** (14-epi lyngbyatoxin; center left) (Jiang, et al., 2014). Teleocidin B is converted from **1** catalyzed via the tleD methyltransferase 1,2-hydride shift of the **1** prenyl tail leading to an *Si*-face attack and cyclization of the prenyl tail to the indolactam-V benzene ring (Awakawa, et al., 2014).

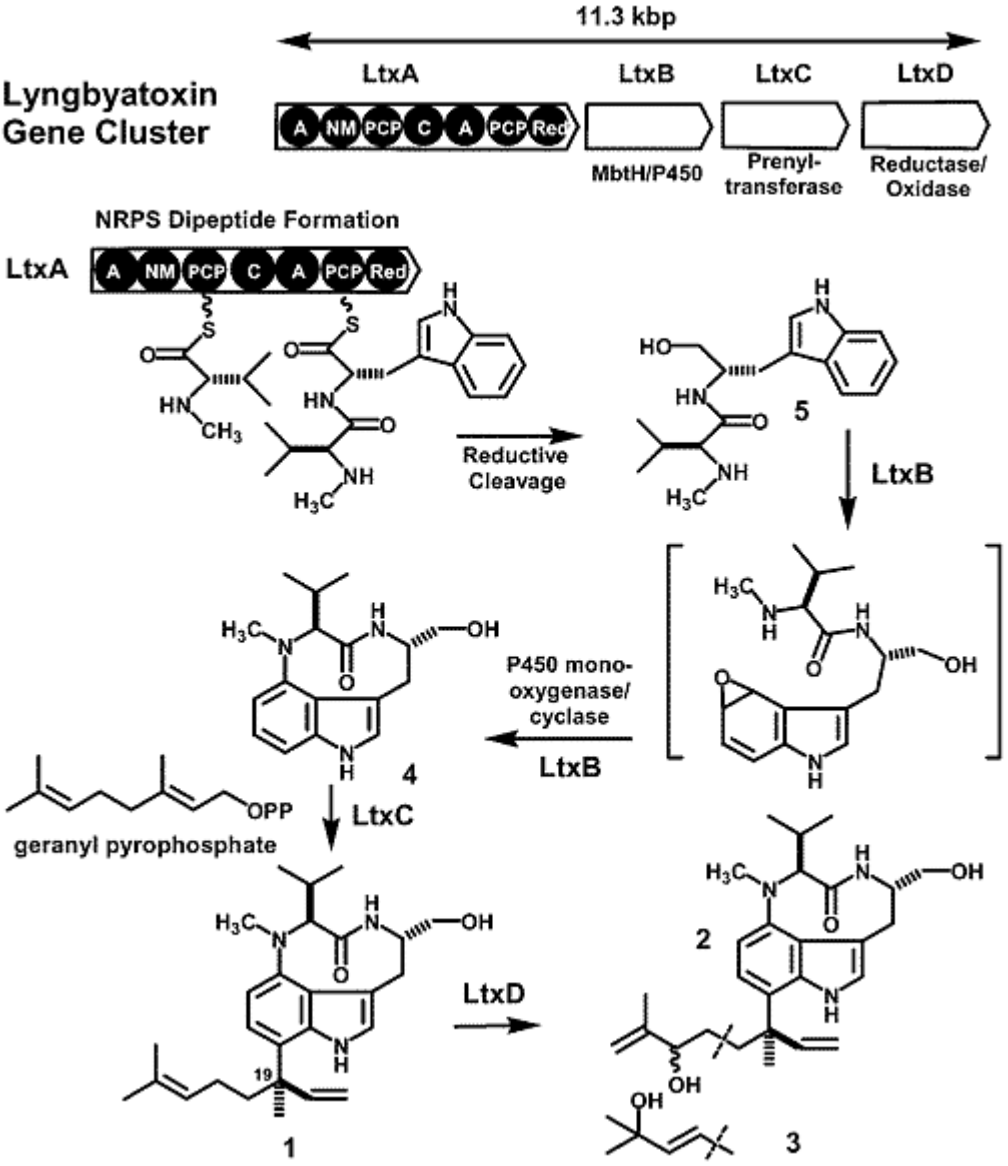

Figure 4. Proposed biosynthesis of lyngbyatoxins A (1), B (2), and C (3). Indolactam-V substructure (4) biosynthesis included during the biosynthesis and serves as the precursor for lyngbyatoxins A-C. Figure from Edwards and Gerwick (2004).

Specific Aim 2: To analyze the phylogeny of previously unidentified *Streptomyces* isolated from *Styela clava* and to localize the bacteria within the host *Styela clava* tissue, the bacterial genome was sequenced and compared to other *Streptomyces* bacterial genomes in the NCBI Genbank database. Bacterial genes were localized to DNA isolated from specific tissue segments of the tunicate host using techniques that included extraction of tunicate and bacterial DNA and amplification of relevant gene segments using polymerase chain reaction (PCR) based on the results of our investigation of the biosynthetic pathway for **1**. The localization efforts were performed in order to identify where the bacteria were located in the tunicate. The results localized relevant bacteria to the interior fluid of the *Styela clava*, but without significant amplification of the genes required for the biosynthesis of **1** within the tunicate.

II. Methods and Materials

A. Extract Library Preparation

Bacteria were isolated from marine tunicate species collected from Long Island Sound, the Bahamas, and the Republic of Panama. Tunicates were collected either by SCUBA or removed from dock lines. Tunicates were rinsed either in sterile water, or 50:50 ethanol (EtOH):H_2O, followed by rinsing in sterile-filtered sea water two times, prior to homogenization. Homogenated tunicate biomass was then spread onto bacterial isolate agar media (3.3% agar [w/v]; no shaking; room temperature; ambient light/air) with naladixic acid (Acros Organics, New Jersey, USA) (final concentration 20 µg/mL) and cyclohexamide (Sigma Aldrich, St. Louis, MO) (final concentration 80 µg/mL) to reduce growth of fast-growing bacteria and fungi, respectively. Morphologically distinct colonies were isolated on ISP-4 agar media (Difco, Detroit, MI) and cultured in sterile liquid media prior to extraction. Large scale cultures were prepared by fermenting bacterial isolates in sterile marine broth (Difco, Detroit, MI) in a shaking incubator (200 rpm; 30 °C; ambient light/air) for 14 days in 500 mL broth. Once fermentation was completed, bacteria cultures were sonicated using a Fisher FS30 ultrasonic cleaner (Fisher Scientific, Hampton, NH; 42 KHz). Five grams of pre-washed Diaion HP-20 beads (Supelco, Bellefonte, PA) was added to each flask and allowed to shake (135 rpm) at room temperature overnight. Bacterial culture with beads were vacuum filtered, aqueous material eluted with water, and then extracted with consecutive washes of methanol and acetone. The resulting organic material was combined and concentrated *in vacuo* to dryness.

B. Immunomodulatory Assay Screen

For screening and PKC activity investigation, bacterial extracts were tested as described previously (Zhao, et al., 2016). Briefly, 10 µL of compounds (stock concentration of 10 mM in

DMSO; final testing concentration 100 μM in DMSO) or DMSO was added to test plates (Corning 3603) prior to cell addition. Dynabeads coated with anti-CD3 or anti-CD8 monoclonal antibody (Thermo Fisher, Waltham, MA) were washed in experimental saline (ES; 155 mM NaCl, 4.5 mM KCl, 1 mM $MgCl_2$, 2 mM $CaCl_2$, 5 mM HEPES, and 10 mM glucose) according to the manufacturer's protocol, and then resuspended beads were added to cell suspension at a ratio of one bead per cell. One hundred microliters of ES-washed TALL-104 cells (2.5 × 106/mL) were added to each well, mixed with DMSO or synthesized compounds, and incubated at 37 °C for 30 min. TALL-104 cells were prepared as previously described (Zhao, et al., 2016). Ten microliters of stimulation solution (ES supplemented with 20 μM thapsigargin [TG] and/or 1 μM phorbol 12-myristate 13-acetate [PMA], anti-CD3 beads, anti-LAMP) or control solution (ES + 4% DMSO, anti-CD8 beads, anti-LAMP) was added to each well and mixed, and the plate was incubated for an additional 50 min in the dark at room temperature with constant rotation. Plates were fixed with 1% paraformaldehyde and samples were transferred to flow tubes for cytometric analysis. Samples were analyzed at selected time points over 1 hour and the measured responses were normalized to control anti-CD3 levels. Alexa647-conjugated anti-LAMP antibody (0.5 μg/mL final concentration) was purchased from BD Pharmingen (San Jose, CA).

C. Isolation and Identification of Teleocidin A-1

Styela clava tunicate specimens were collected from shallow water dock lines at Avery Point, CT, in May 2011 (41° 18.975 N, 72° 3.647 W) (Figure 5). The bacterium was isolated on sterile ISP Medium 4 agar (37 g/L; BD Difco™), made with Instant Ocean (33 g/L; United Pet Group, Blacksburg, VA) and cultured at room temperature. The morphology of AVP053U2 resembled an actinobacterium, with a yellow base and green and white spores. AVP053U2 was subjected to whole genome sequencing (described below) and determined to be a new strain from

the genus *Streptomyces* (deMayo, et al., in press). *Streptomyces* sp. AVP053U2 was cultured for 14 days in 500 mL of sterile marine broth (200 rpm; 30 °C; ambient light/air) and chemically extracted.

For extraction, pre-washed HP-20 Diaion beads (Supelco) were added to bacterial cultures and left to incubate at room temperature overnight shaking at 135 RPM. Following overnight incubation, beads were washed with H_2O (500 mL), methanol (MeOH) (1 L), and acetone (500 mL). The MeOH and acetone layers were combined and concentrated *in vacuo*. The organic extract was initially fractionated via C_{18} reversed-phase (RP) solid-phase extraction (SPE) chromatography (Supelco) using a stepwise MeOH:H_2O gradient as follows: 10% MeOH:H_2O (fraction A), 25% MeOH:H_2O (fraction B), 50% MeOH:H_2O (fraction C), 75% MeOH:H_2O (fraction D), and 100% MeOH (fraction E). A final wash of 100% acetone (fraction F) was used to clean any remaining material from the column. All fractions were concentrated to dryness *in vacuo*. Fractions were then subjected to gradient liquid chromatography–mass spectrometry (LC-MS) characterization on an Agilent 6130 ESI single quadrupole mass spectrometer comprised of an Agilent G1311 quaternary pump, G1322 degasser, and G1315 diode array detector and coupled to an Agilent 1200 series high-performance liquid chromatography (HPLC) system (Agilent Eclipse XDB-C_{18}; 5 µm; 4.6 × 150 mm column). Initial LC-MS was performed using a 40%–100% ACN:H_2O gradient (0.1% formic acid) solvent system for 30 min.

During secondary screening, fraction E exhibited the most potent activity and was further investigated. Compound **1** (1.4 mg) was isolated by C_{18} RP-HPLC using an isocratic method of 35% H_2O and 65% ACN (Agilent Eclipse XDB-C18; 5 µm; 4.6 × 150 mm column; 1 mL/min flow rate, rt 12 minutes). Nuclear magnetic resonance (NMR) spectra of **1** were collected in DMSO-*d*6 on a Varian INOVA 600 MHz instrument including ^{1}H, COSY, HSQC, and HMBC.

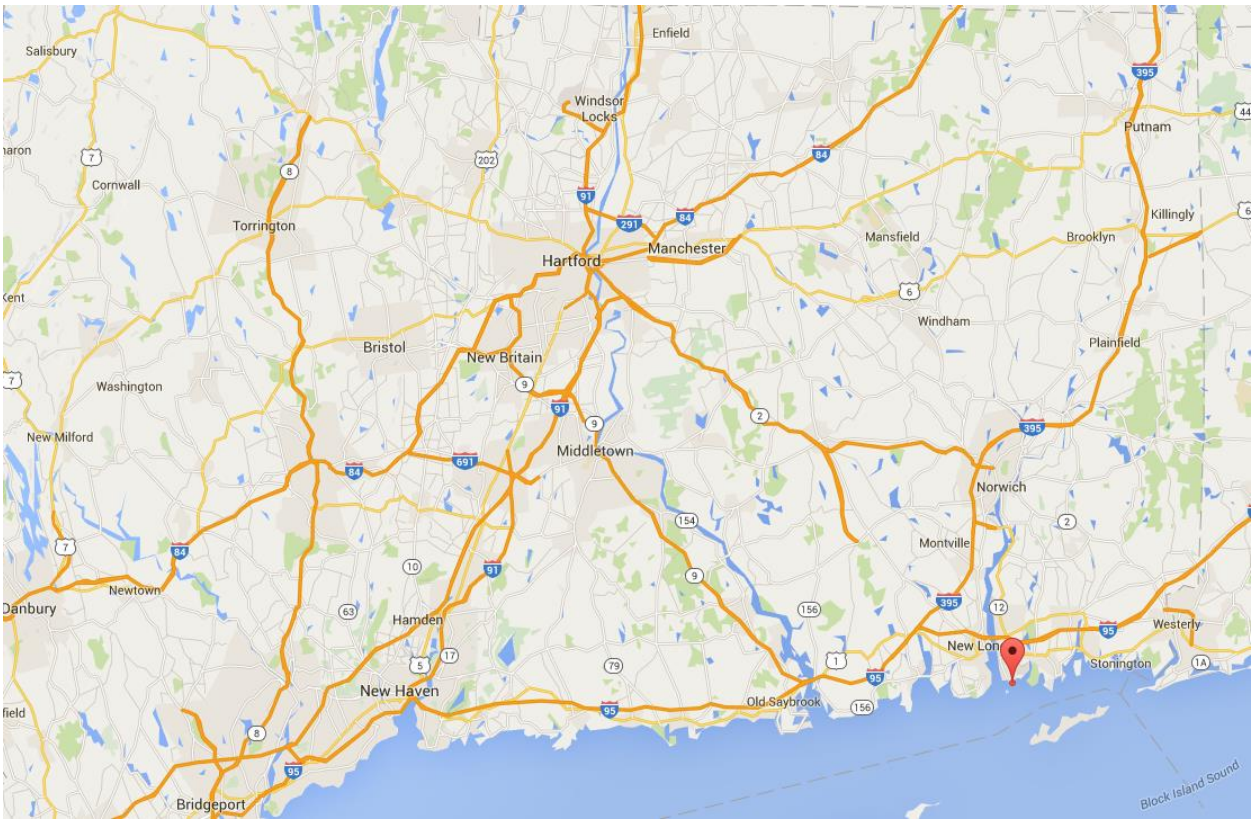

Figure 5. Map of southeastern Connecticut. Collection location was at University of Connecticut Avery Point campus (Groton, CT) (Google Maps, 2016).

NMR spectra for ^{13}C experiments were collected on a 500 MHz Bruker AVANCE at 125 MHz. Chemical shifts were reported in δ units (ppm) using DMSO-d_6 as the internal standard for signals. High resolution mass spectrometry (HRMS) was performed at the University of Connecticut Mass Spectrometry Facility on an AccuTOF (JEOL) using a DART (IonSense) ionization source. Optical rotation experiments were collected on a JASCO P-2000 polarimeter (*c* 0.13 g/100mL, MeOH, 26 °C). CD spectra was collected on an Applied Photophysics Pi-star 180 circular dichroism spectrapolarimeter (Leatherhead, Surrey, UK) (*c* 0.5 mg/mL, MeOH, 21 °C).

D. DNA Extraction and Genome Sequencing

Bacterial DNA. Colonies of sporulated bacteria were cultured on Difco ISP Medium 4 agar as described above, removed with sterile loops into sterile 1.5 mL microcentrifuge tubes (Eppendorf), and DNA was extracted using a Wizard Genomic DNA Purification Kit (Promega Corporation, Madison, WI) according to the manufacturer's protocol. The Illumina TruSeq Nano DNA Library Preparation Kit was used to fragment DNA (200 ng), attach adapter sequences, and size selected, according to manufacturer's protocol (UConn MARS facility). Libraries were validated and an Agilent Bioanalyzer High Sensitivity chip was used to calculate mean insert length (UConn MARS facility). Libraries were sequenced on the Illumina MiSeq using v2 2x250 base pair kit, assembled with A5-miseq pipeline v20140113 (Coil, et. al. 2015), checked for contamination with Blobology pipeline (Kumar, et al., 2013), and annotated with Prokka v1.10 (Torsten, 2014) (Jonathan Klassen, UConn Dept. of Molecular and Cellular Biology). Phylogenetic analysis of the bacteria was completed using the ORFcor bioinformatics pipeline (Klassen and Currie, 2013) (Jonathan Klassen, UConn Dept. of Molecular and Cellular Biology).

Tunicate DNA. Styela clava individuals were collected from shallow water dock lines at Avery Point, CT, (41° 18.975 N, 72° 3.647 W). Upon collection, individual tunicates were rinsed

with seawater and Millipore filtered DI water or 50:50 EtOH:H_2O to sterilize the outer surface of the tunic, leaving internal bacteria embedded within the tissue, and relaxed in a solution of 10% menthol in DI water. Tunicates were transported back to the lab where tissue samples were dissected. The tissue dissections included tunic (T), internal gut (G), and internal fluid material that was drained and collected upon initial incision (F) (Figure 6).

Following dissection, tunicate specimens were frozen at -20 °C until DNA extraction. DNA extractions were performed based on a previously published protocol for isolating DNA from tunicates (Schmidt and Donia, 2009). Tunic tissue samples were divided into small pieces approximately 4-5 mm^2 in size. Organ samples were lyophilized and ground together using a mortar and pestle and suspended in 1X TE buffer (10 mM Tris-Cl, 1 mM EDTA, pH 8.0). Lysozyme was added to the buffer-homogenate solution to a final concentration of 2 mg/mL and incubated at 30 °C for 30-60 minutes. (Ethylenediaminetetraacetic acid) EDTA was added to a concentration of 0.1M, Proteinase K solution was added to a final concentration of 0.2 mg/mL, and the homogenate was incubated at 30 °C for 5 minutes. 10% Sodium dodecyl sulfate (SDS) solution was added to a final concentration of 1% and the homogenate solution was incubated tilted at 90° at 37 °C overnight. Ten percent (v/v) NaCl solution (5M) and eight percent (v/v) CTAB solution [10% CTAB (hexadecyltrimethyl ammonium bromide) in 0.7 M NaCl] was added to the solution and incubated for 20 to 60 minutes at 65 °C. To extract DNA, 500 µL of homogenate solution was aliquoted into sterile 1.5 mL centrifuge tubes, mixed with 420 µL of both deuterated chloroform and saturated phenol solution, and vortexed to mix. Solution was centrifuged at 17,000 x g for ten minutes and the top (aqueous) layer was removed. Aqueous layer was mixed with 0.1 volumes of 3 M sodium acetate and 0.6 volumes of ice-cold isopropanol. Tube was mixed by inversion until DNA precipitated and centrifuged at 17,000 x g for two minutes to pellet the DNA.

Figure 6. Photos of dissected *Styela clava*: A) whole *Styela clava* prior to dissection; B) dissected tunic tissue (T) and C) dissected gut/GI tract tissue (G). Not pictured: internal fluid (F).

The supernatant was aspirated and the DNA pellet was washed with 300 µL of 70% EtOH. The tube was centrifuged at 17,000 x g for two minutes to re-pellet the DNA, EtOH was aspirated, and the DNA was left to dry for ten minutes. Dried DNA was resuspended in TE buffer and measured for concentration and purity via NanoDrop (ThermoFisher, USA). Tunicate internal fluid (F) was filtered onto 0.22 µm nitrocellulose filters (EMD Millipore, Darmstadt, Germany) and DNA was extracted using a MoBio PowerWater DNA Isolation Kit (MoBio Laboratories, Carlsbad, CA, USA) according to the manufacturer's protocol. DNA concentration and purity was quantified using a NanoDrop (ThermoFisher, USA).

Primer Design. Base pair sequences for each protein gene involved in teleocidin biosynthesis and for the 16S rRNA gene were identified and primer pairs were designed for a conserved region within each domain for future PCR amplification experiments. Primers were designed for amplification of a segment from the 16S rRNA gene specific for *Streptomyces* related organisms based on the sequencing results mentioned previously, and for amplification of a segment from the 18S rRNA gene specific for *Styela clava*. Custom PCR primers were designed for amplification of *Streptomyces* 16S rDNA, *Styela clava* 18S rDNA, and teleocidin biosynthesis gene segments using Primer3 (v 4.0.0) primer identifier software (Untergasser, et al., 2012) (Koressaar and Remm, 2007) (Table 1). Parameters for primer identification included primer size (18-23bp), melting temperature (57.0-62.0 °C), and GC% (30.0-70.0). Primers 27F and 1391R were used for universal amplification of 16S rRNA gene (Frank, et al., 2008) (Beckers, et al., 2016). Amplicon length was 1.2 kbp. Primers designed specifically for the *Streptomyces* 16S rRNA sequence were produced based on the genome of *Streptomyces* sp. AVP053U2. Primers for teleocidin biosynthesis were designed for a conserved, easily amplifiable region of each DNA segment involved in teleocidin biosynthesis identified from the genome of *Streptomyces* sp.

AVP053U2. Primer specificity was validated using Primer-BLAST. Amplicon lengths were designed as follows: *tleA* – 201 bp, *tleB* – 250 bp, *tleC* – 223 bp, MbtH-like protein – 182 bp. Primers for amplification of 18SrDNA were designed based on sequence for *S. clava* 18S rRNA (Genbank Accession: AH001758). Amplicon lengths were designed for 235 bp.

Polymerase Chain Reaction. PCR reactions were prepared with GoTaq Green MasterMix (Promega Corporation, Madison, WI, USA) according to the manufacturer's instructions. Final concentrations of dNTPs, forward and reverse primers, and $MgCl_2$ were 200, 0.4 μM, and 1.5 mM, respectively. Master Mix was prepared in a proprietary buffer at pH 8.5 combined with yellow and blue dyes for visualization during gel electrophoresis. Varying concentrations of template DNA were added in order to optimize amplification and visualization (Table 2).

Reaction protocols for PCR experiments to amplify bacterial 16S rDNA were as follows: 2 minutes of denaturing at 96 °C, followed by 30 cycles of 45 seconds at 96 °C (denaturing), 30 seconds at 56 °C (annealing), and 2 minutes at 72 °C (elongation), and a final extension for 5 minutes at 72 °C. The reaction protocol for PCR experiments for amplifying eukaryotic 18S rDNA segments were performed as follows: 2 minutes of denaturing at 95 °C, followed by 35 cycles of 1 minute at 95 °C (denaturing), 1 minute at 40 °C (annealing), and 1.5 minutes at 72 °C (elongation), and a final extension for 7 minutes at 72 °C. PCR Products were analyzed via agarose gel electrophoresis stained with ethidium bromide. Photographs of the stained agarose gel PCR products were collected using a UVP GelDoc-It 300 Imaging System (Upland, CA, USA). PCR reaction positive controls for amplification of 18S rDNA included DNA extracted from *S. clava*. Positive controls for 16S rDNA PCR reactions were DNA from *Streptomyces* sp. AVP053U2 and *E. coli*. Negative control for gut and tunic tissue DNA reactions was 1X TE Buffer. Negative control for fluid and environmental water reactions was solution PW6 (MoBio laboratories,

Carlsbad, CA, USA). PCR products were cleaned using a Promega Wizard SV Gel/PCR Clean-up Kit (Promega Corporation, Madison, WI, USA) according to the manufacturer's instructions. Clean double-stranded PCR products were analyzed for concentration and purity via NanoDrop (ThermoFisher, USA) for the ratio of light absorbance at 260 nm and 280 nm (Glasel, 1995), and Sanger sequenced for BLAST analysis (megablast; expect threshold: 10; match/mismatch scores: 1, -2; linear gap costs) to ensure successful amplification of the intended sequence(s) (Kendra Maas, UConn MARS Facility).

Table 1. Primer sequences for PCR experiments. The primer sequences were used for amplification of housekeeping genes identified in tunicate and bacterial DNA. "*MbtH*-like gene" refers to the annotation for the fourth gene involved in teleocidin biosynthesis.

Primer Name	Primer sequence (5'-3')	Target DNA Sequence
27F	AGAGTTTGATCCTGGCTCAG	16S rDNA
1391R	GACGGGCGGTGTGTRCA	16S rDNA
AVPfor3	AAGTGACGGTACCTGCAGAA	16S rDNA
AVPrev3	TCACCGCTACACCAGGAATT	16S rDNA
S.clava18Sfor	ATTCTTGGATCGGCGGAAGA	18S rDNA
S.clava18Srev	ATTGCTCAATCTCGTGTGGC	18S rDNA
tleAfor2	TCAGGACCTATCGTTCGAGA	*tleA*
tleArev2	AGGCTCAGTGAAAGGTCGAA	*tleA*
tleBfor2	GATGACGGAGGAGGAGATCG	*tleB*
tleBrev2	GGGTGAACAGGACGTACAGA	*tleB*
tleCfor2	GGCATGCCTTTCGAAGTATC	*tleC*
tleCrev2	CGTGGGAGAGCGAGAAGTAT	*tleC*
MbtHfor2	CTTTCTCGGTGCTGGTCAAC	*MbtH*-like gene
MbtHrev2	AGAACCGGTCGTAGTGCTC	*MbtH*-like gene

Table 2. Template DNA used for PCR experiments. PCR reactions were optimized and visualized via gel electrophoresis. DNA quantified via NanoDrop UV detection.

Template DNA	Primers used	Total amount of DNA per 50 μL reaction (ng)
AVP053U2	AVP16Sfor3/AVP16Srev3	707
AVP053 – Fluid	AVP16Sfor3/AVP16Srev3	25
AVP053 – Fluid	27F/1391R	25
AVP053 – Tunic tissue	SCLAVA18Sfor/SCLAVA18Srev	11
Sea Water	AVP16Sfor3/AVP16Srev3	9
Sea Water	27F/1391R	9
E. coli	27F/1391R	10

III. Results

A. Screening of Tunicate-Associated Bacterial Extracts

A library of 294 extracts prepared from tunicate-associated bacteria was screened for their ability to enhance or inhibit CTL granule exocytosis. Using the assay described by Zhao et. al. (2016) yielded a hit for stimulation of lytic granule exocytosis (Figure 7A). Treatment with the extract enhanced lytic granule exocytosis by nearly three times the physiological level. The extract had no effect on cells that were not pre-stimulated by beads with anti-CD3 antibody. Repetition of the experiment confirmed the granule exocytosis augmenting effect.

The extract was fractionated using a reversed-phase solid phase extraction (SPE) column (Supelco, Bellefonte, PA) (Figure 8), and the activity was examined for each of the individual fractions (Figure 7B). Upon initial screening, fraction E was the most potent prefraction, yielding a five-fold enhancing effect of cells stimulating by CD3 beads as measured cytometrically for anti-LAMP fluorescence. This result is comparable to treatment with TG and PMA on CD3 stimulated cells. Fluorescence values for cells stimulated with anti-CD3 antibodies and fraction E reached 100 relative fluorescence units (RFU), while cells stimulated with anti-CD3 antibodies combined with TG and PMA reached 120 RFU. Fraction E was chosen for compound isolation via RP-HPLC as a result of the easily distinguishable peaks. The peak eluting at a retention time of 12 min was isolated as a pure compound as described below, and coded as E1 (Figure 9), which was found to enhance lytic granule exocytosis with an EC_{50} of approximately 1 nM (Figure 7C).

To determine the mechanism of action for lytic granule exocytosis as a result of treatment with E1, cells were treated for 90 minutes with either E1 or PMA in order to compare levels of enhancement. PKC activity enhancement was investigated further because although calcium influx and activation of PKC and ERK are required for CTL granule exocytosis (Pores-Fernando and

Zweifach, 2009), limited exocytosis was observed in cells not treated with beads when treated with E1. Activity-guided fractionation of the active extract led to the isolation of E1, exhibiting potent stimulatory activity on the PKC pathway independent of calcium influx activity. Imaging of live cells using the calcium-sensitive probe Fura-2 confirmed granule exocytosis activity regardless of intracellular calcium concentration. Dose-response measurements of PKC activity identified the enhancement levels of E1 and PMA across three concentrations ranging from 0.01 to 200 nM (Figure 7D). Furthermore, treatment with E1 resembled that of treatments whose effects occur independent of intracellular calcium concentration (Figure 10). Fits to the Hill equation indicate that E1 activated PKC with an EC_{50} of 6.9 nM, almost as potent as PMA (EC_{50} = 3.6 nM).

B. Identification of Teleocidin A-1

Structure elucidation of E1 utilized a series of one-dimensional (1D) and two-dimensional (2D) NMR experiments (Figures 11-15, Table 3) in addition to mass spectrometric analysis. HRMS of E1 identified a molecular ion peak at *m*/*z* 438.3112 [M + H]+ (Figure 16) consistent with the formula $C_{27}H_{39}N_3O_2$. The molecular formula was indicative of ten degrees of unsaturation. Partial structure elucidation and comparison with literature NMR data (Jiang, et al., 2014) led us to identify E1 as a derivative of teleocidin. The ^1H spectra indicated several aromatic signals around 7.0 ppm consistent with a heterocyclic aromatic compound. In addition, two distinct downfield signals highlight heterocyclic amido and/or hydroxyl protons. Two pairs of signals appeared as a doublet of doublets, indicating close proximity to stereogenic carbons with enantiotopically distinct protons with shifts at δ_H 2.93 and δ_H 3.04 ppm, and δ_H 5.03 and δ_H 5.09 ppm. ^1H-^{13}C HSQC correlated these two proton signals to carbons with signals at δ_C 34.1 and δ_C 112.2 ppm respectively. The downfield shifts of the latter proton and carbon signals indicated sp^2 hybridization. Further analysis of the downfield proton signals at δ_H 5.03 and δ_H 5.09 via ^1H-^1H COSY showed no

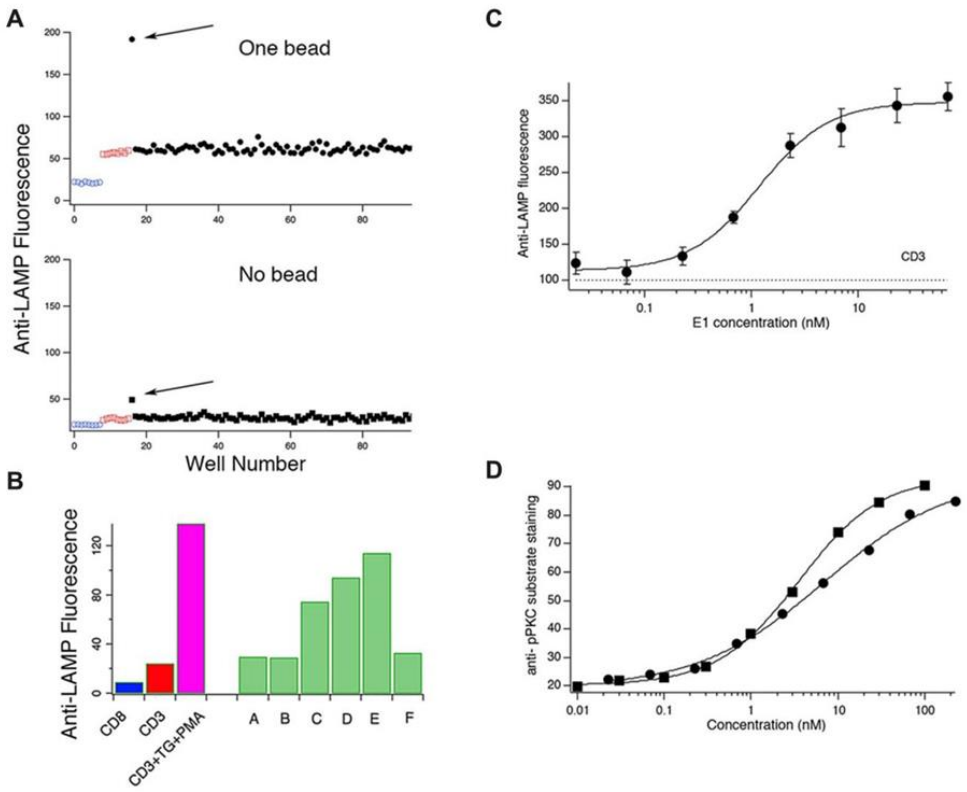

Figure 7. Detection and activity-guided isolation of an exocytosis-enhancing PKC-activating compound. (A) Screening of bacterial extracts measuring for anti-LAMP fluorescence. Red spots represent cells stimulated with CD3 beads only. Blue spots represent cells stimulated with CD8 beads only. Black spots represent cells treated with CD3 beads and bacterial extracts. The highlighted black spot represents the most successful hit and was discovered to contain **1**. (B) Prefractions of the hit extract were further examined in the same assay as in **A**. Anti-LAMP fluorescence values of cells treated with prefractions A-F are compared to CD8 (blue), CD3 (red), and CD3+TG+PMA (pink) controls. (C) Dose-response measurement of the first compound isolated from prefraction E measuring for anti-LAMP fluorescence. (D) Comparisons of dose-response measurements for anti-LAMP fluorescence between cells treated with E1 (circles) and PMA (squares). Experiments were conducted three times in C and twice in D (Zhao, et al., 2016).

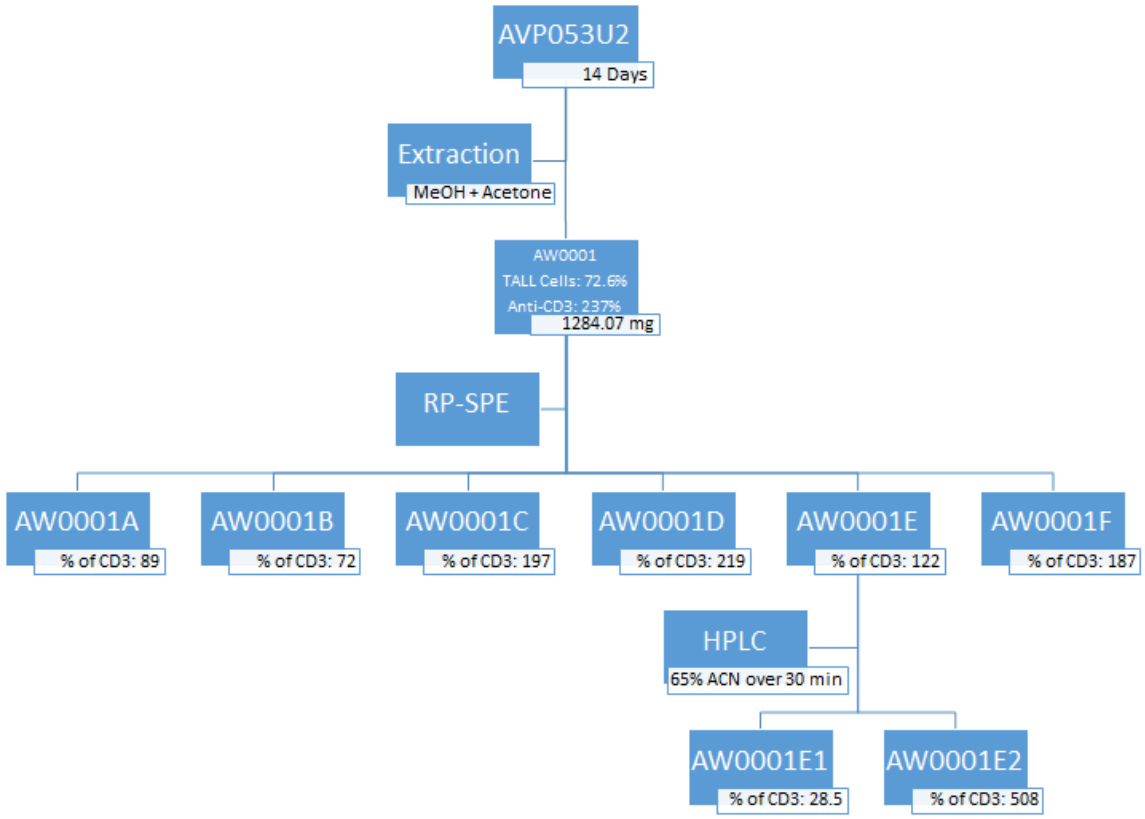

Figure 8. Chemical structure schematic. Organic solvents used for chemical extraction (MeOH and acetone) and percent CD3 bead enhancement for each extract and fraction tested are included. AVP053U2 was cultured for 14 days prior to chemical extraction overnight and fractionation into six prefractions. Fraction E was subject to HPLC using an isocratic method of 65% acetonitrile over 30 minutes to elute the peak of interest, E1, at 12 minutes. RP-SPE: reverse-phase solid phase extraction; HPLC: high performance liquid chromatography.

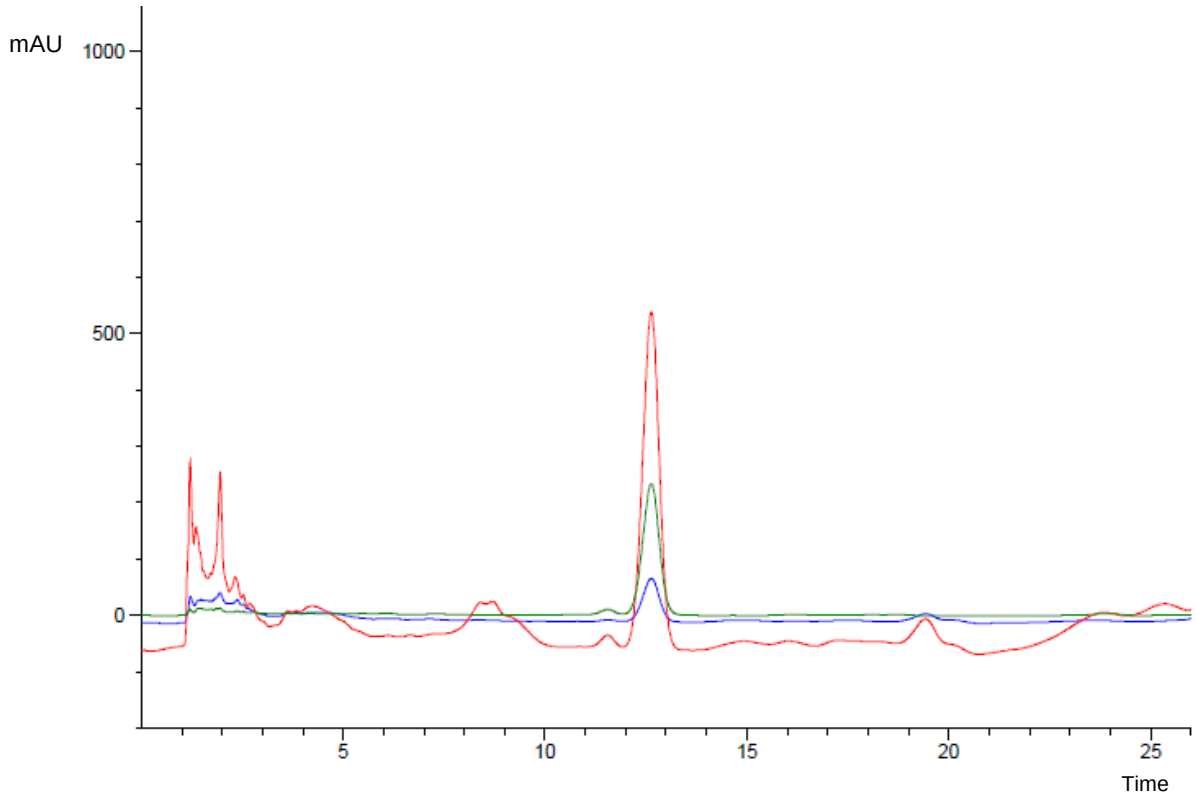

Figure 9. LC chromatogram of Fraction E containing teleocidin A-1. HPLC chromatogram of fraction E with the peak E1 eluting at approximately 12 minutes. Method developed as 65:35 ACN:H_2O with 100 µL solution injected at 2 mg/mL. Blue trace represents absorbance at 254 nm, red trace represents absorbance at 209 nm, and green trace represents absorbance at 299 nm. Absorbance measured in mAU.

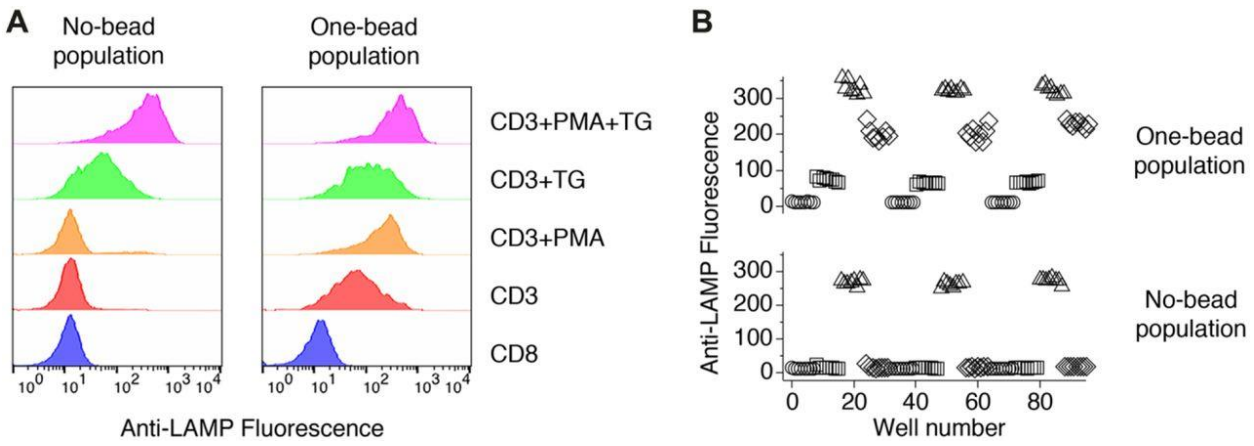

Figure 10. Treatment with anti-CD3 beads provide additional capacity for lytic granule exocytosis. (A) Histograms of anti-LAMP fluorescence for the conditions indicated. Results from treatment with TG, which acts through increase of calcium influx, are similar regardless of the pre-stimulation with anti-CD3 beads. Treatments with PMA, which stimulate granule exocytosis through PKC activation (independent of calcium influx), yield higher anti-LAMP fluorescence values. (B) Plots of the geometric mean of anti-LAMP fluorescence from a 96-well plate containing cells and anti-CD8 beads (circles), anti-CD3 beads (squares), anti-CD3 beads + PMA (diamonds), and anti-CD3 beads + TG + PMA (triangles). Responses from cells assessed as bound to beads by scatter are shown on top. Responses from cells that are not bound to beads are on the bottom. Experiments were conducted more than three times. TG and PMA were used at final concentrations of 2 μM and 100 nM, respectively (Zhao, et al., 2016).

correlation with other proton signals, indicating a terminal methylene adjacent to an enantiotopic proton. Upfield carbon signals at δ_C 17.2 and δ_C 24.2 ppm correlated with singlet proton signals at δ_H 1.38 and δ_H 1.42 ppm respectively. The singlet splitting pattern of these proton signals indicate two terminal methyl protons both adjacent to an *sp*^{2} hybridized quaternary carbon center. ^{1}H-^{13}C HMBC spectroscopy confirmed the proximity of the signals at δ_H 1.38 and δ_H 1.42 ppm to a quaternary carbon signal at δ_C 130.4 ppm. Additional upfield proton signals at δ_H 0.51 and δ_H 0.81 ppm were both shown to correlate to a proton signal at δ_H 2.44 ppm with doublet splitting patterns, indicating a dimethyl substituted methyl group. Further ^{1}H-^{13}C HSQC analysis identified proton signals at δ_H 3.35 and 3.4 ppm and contain multiplet splitting patterns that correlate to a carbon signal at δ_C 63.9 ppm. The downfield tendencies for both the proton and carbon signals indicate proximity an electronegative heteroatom. In addition, examination of the ^{1}H-^{13}C HSQC spectra identifies one far downfield proton signal that appears not to correlate with a carbon signal, which can attributed to an electronegative heteroatom. ^{1}H-^{1}H COSY analysis indicated that the only proton signal which correlates to the furthest downfield proton signal at δ_H 9.86 ppm belongs to a proton signal at δ_H 6.93 ppm identifying proximity to an electronegative heteroatom. Finally, analysis of the ^{1}H-^{13}C HMBC spectra identifies two multiple-bond carbon correlations to the proton signal at δ_H 9.86 ppm, indicating that two carbons are adjacent to the heteroatom whose proton signal appears at δ_H 9.86 ppm. These results indicate that the heteroatom is likely a nitrogen.

To determine the absolute stereochemistry of E1, optical rotation and circular dichroism (CD) experiments were performed. Both experiments were utilized in order to confirm the stereospecific orientation of all three predicted chiral centers. Optical rotation results indicated a degree of rotation of $[\alpha]_D^{20} = -35°$, consistent with literature values of teleocidin A-1 (Jiang, et al., 2014). For additional confirmation of the configuration of E1, CD spectra data were obtained

in MeOH as follows: $[\theta]_{230} = -655$, $[\theta]_{234} = 4892$, $[\theta]_{259} = -24189$, $[\theta]_{314} = -1290$, and $[\theta]_{328} = -3183$ (Figure 17), confirming that compound E1 is consistent with the planar and stereo-structure of teleocidin A-1 (Jiang, et al., 2014).

C. Bacterial DNA and Genome Sequencing

Investigation of the whole genome associated with the bacteria was of particular interest after isolating and identifying **1**. The structure of **1** is consistent with metabolites produced from sophisticated non-ribosomal peptide synthetase (NRPS), terpene, and polyketide synthase (PKS) pathways. As a result, the relevant biosynthetic gene clusters associated with the production of **1** were identified, in addition to other biologically relevant gene sequences. Genomic DNA was extracted from a pure culture of bacteria and sequenced as described above. Whole genome sequencing identified the bacterium as a novel strain of *Streptomyces* sp and was delineated AVP053U2. Bi-directional average nucleotide identity (ANI) calculated to be 99.68% identical to *Streptomyces* sp. TP-A0873 (NCBI Accession Number: BBNN00000000) (Goris, et al., 2007). The genome was sequenced to 153X coverage containing 7,759,417 nucleotides with 183 scaffolds. The total GC content was identified as 71.85% with $N_{50} = 137{,}942$ bp.

The sequence was examined using antiSMASH 3.0.4 (Antibiotics and Secondary Metabolite Analysis Shell) to identify relevant secondary metabolite gene clusters (Weber, et al., 2015). Forty-six putative clusters were identified with six sharing 100% identity with previously reported clusters, including those for teleocidin-B, isorenieratene, albaflavenone, antimycin, γ-butyrolactone and ectoine biosynthesis. The remaining clusters included 11 NRPS, seven T1-PKS, six terpene, three lantipeptide, two NRPS/T1-PKS, two siderophore, one each of amgylccycl/NRPS, T1-PKS/transAT-PKS/NRPS, terpene/T2-PKS, indole/NRPS, melanin, NRPS/lantipeptide, butyrolactone/T1-PKS, butyrolactone, nucleoside, ectoine, bacteriocin,

Table 3. NMR chemical shifts and splitting patterns for peaks in ^{1}H and ^{13}C spectra. Proton and carbon peaks identified are in Figure 11. All shift units reported in ppm. Carbon numbers correlate to labeled diagram for **1** in Figure 3.

No.	δ_C	δ_H	Splitting Pattern
1	17.2	1.38	s
2	19.5	0.51	d
3	21.4	0.81	d
4	22.9	1.57	m
		1.79	m
5	25.4	1.58	s
6	24.2	1.42	s
7	28	2.44	m
8	32.6	2.77	s
9	34.1	2.93	dd
		3.04	dd
10	38.4	1.76	m
		1.96	m
11	42.9		
12	55.6	3.98	m
13	63.9	3.35	m
		3.4	m
14	70.3	4.24	d
15	105	6.35	d
16	112.2	5.03	dd
		5.09	dd
17	112.8		
18	118.6		
19	119.6	6.79	d
20	122.5	6.93	d
21	121.6		
22	124.6	5.01	m
23	130.4		
24	136		
25	145.7		
26	146.3	6.12	m
27	171.7		

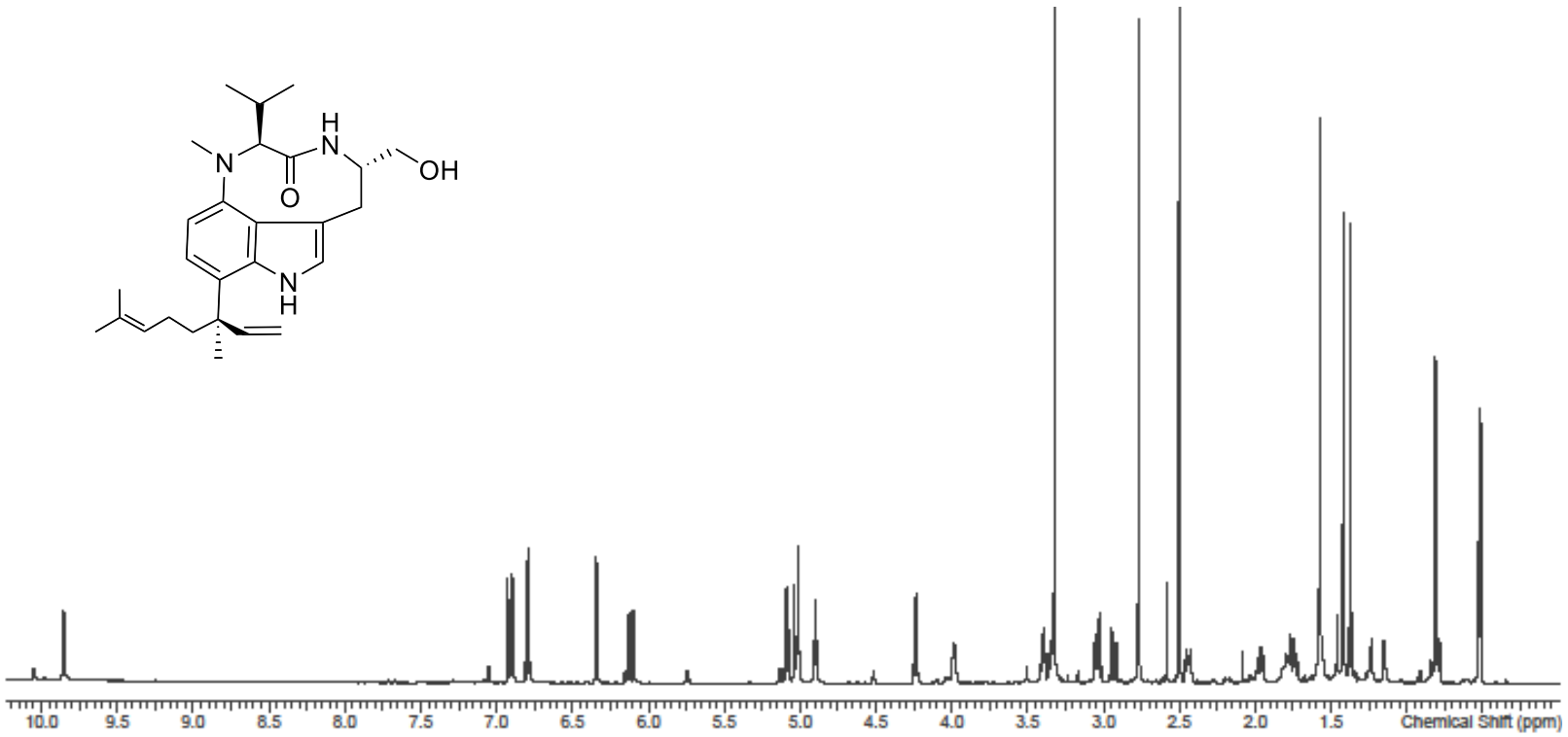

Figure 11. ^{1}H NMR spectra of **1** (teleocidin A-1). Spectra was collected at 600 MHz in DMSO-*d*6.

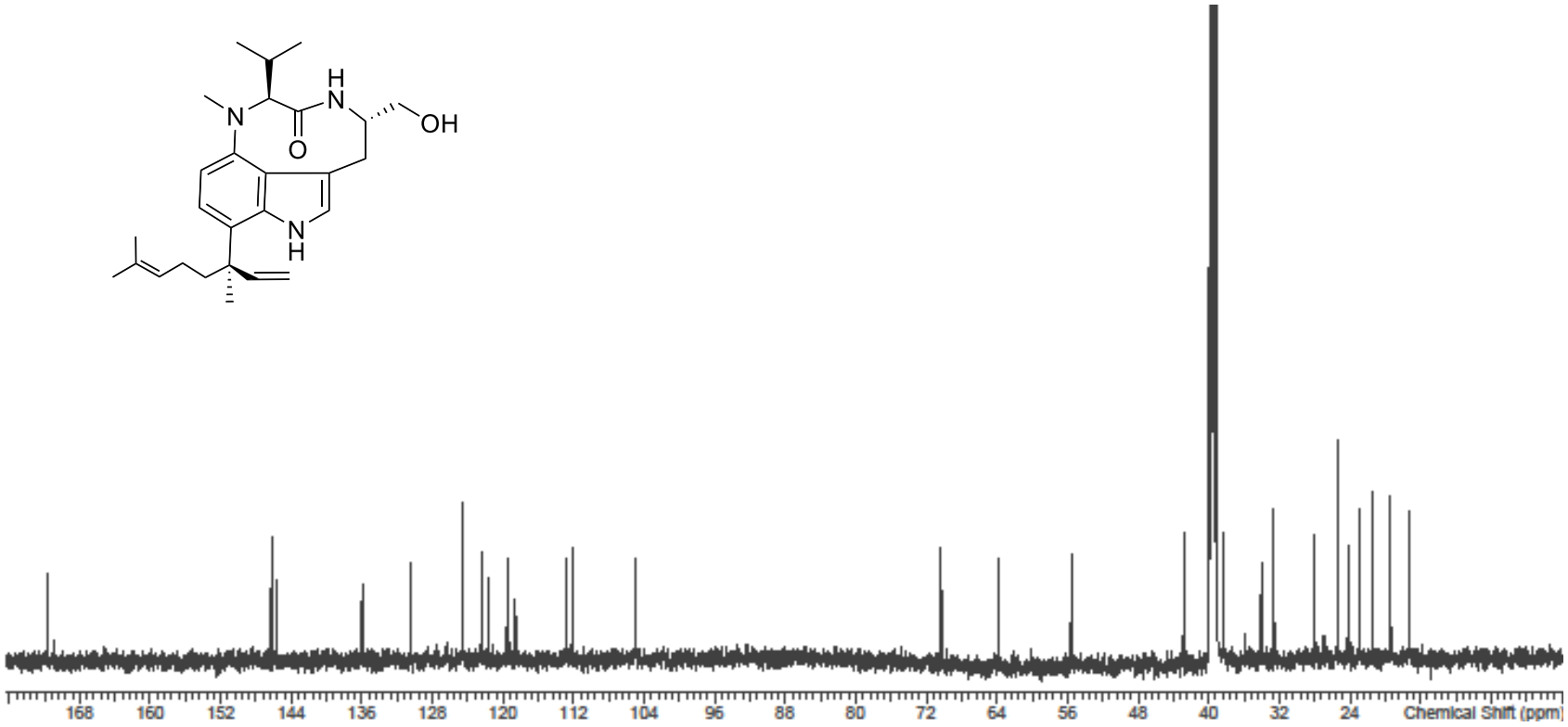

Figure 12. ^{13}C NMR spectra of **1** (teleocidin A-1). Spectra was collected at 125 MHz in DMSO-*d*6.

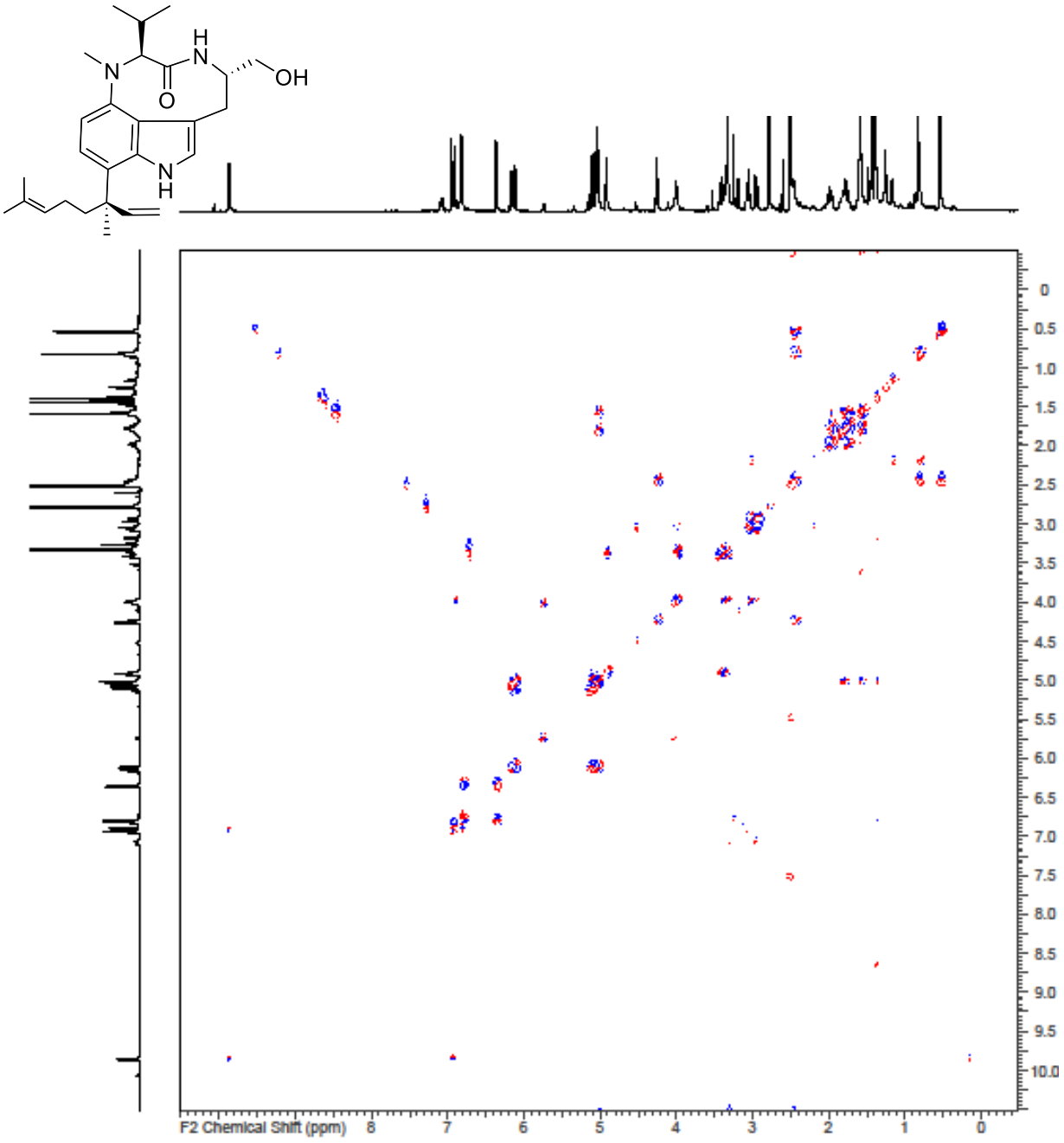

Figure 13. ^{1}H-^{1}H COSY NMR spectra of **1** (teleocidin A-1). Spectra was collected in DMSO-*d*6.

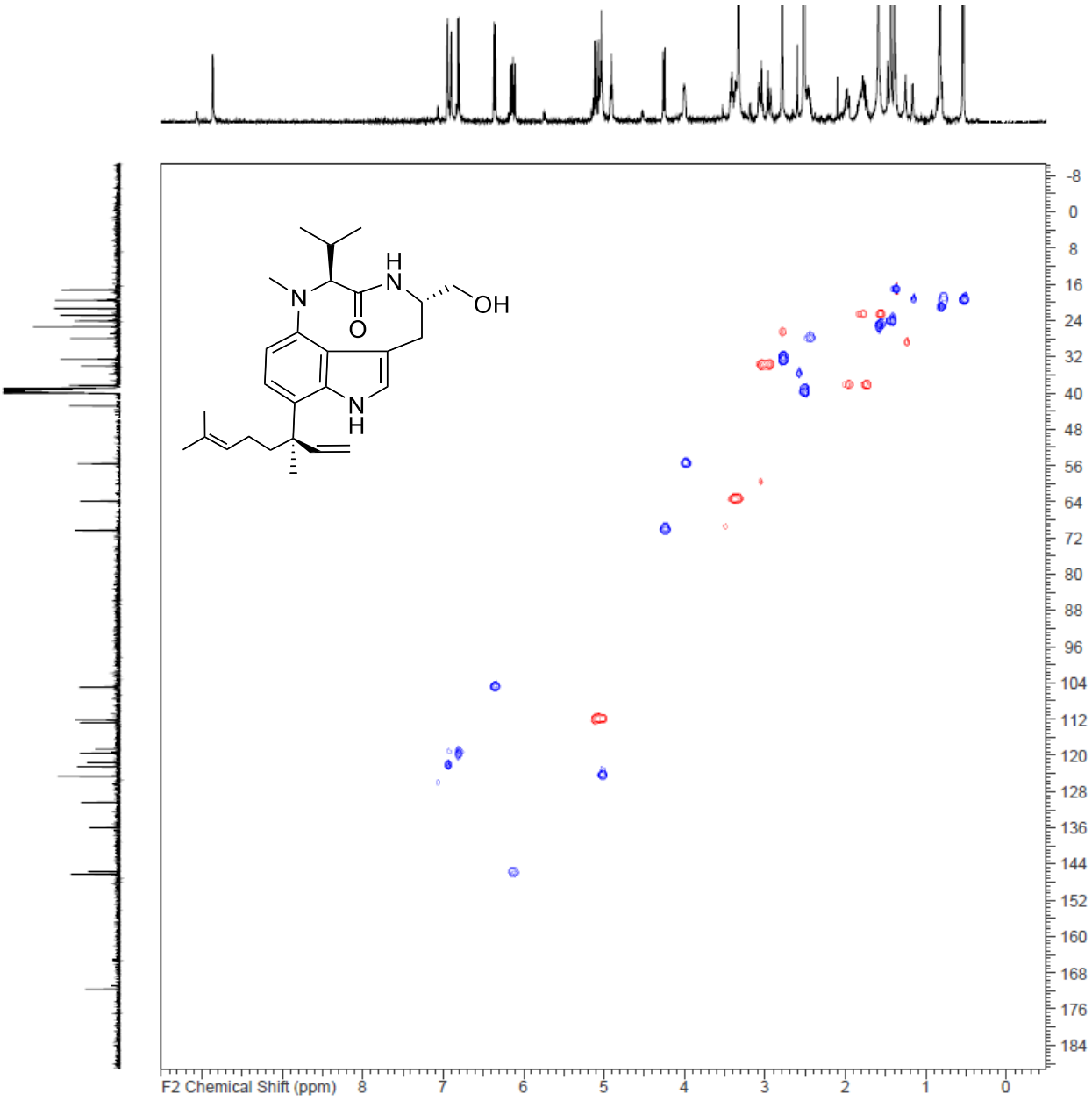

Figure 14. ^{1}H-^{13}C HSQC NMR spectra of **1** (teleocidin A-1). Spectra was collected in DMSO-*d*6.

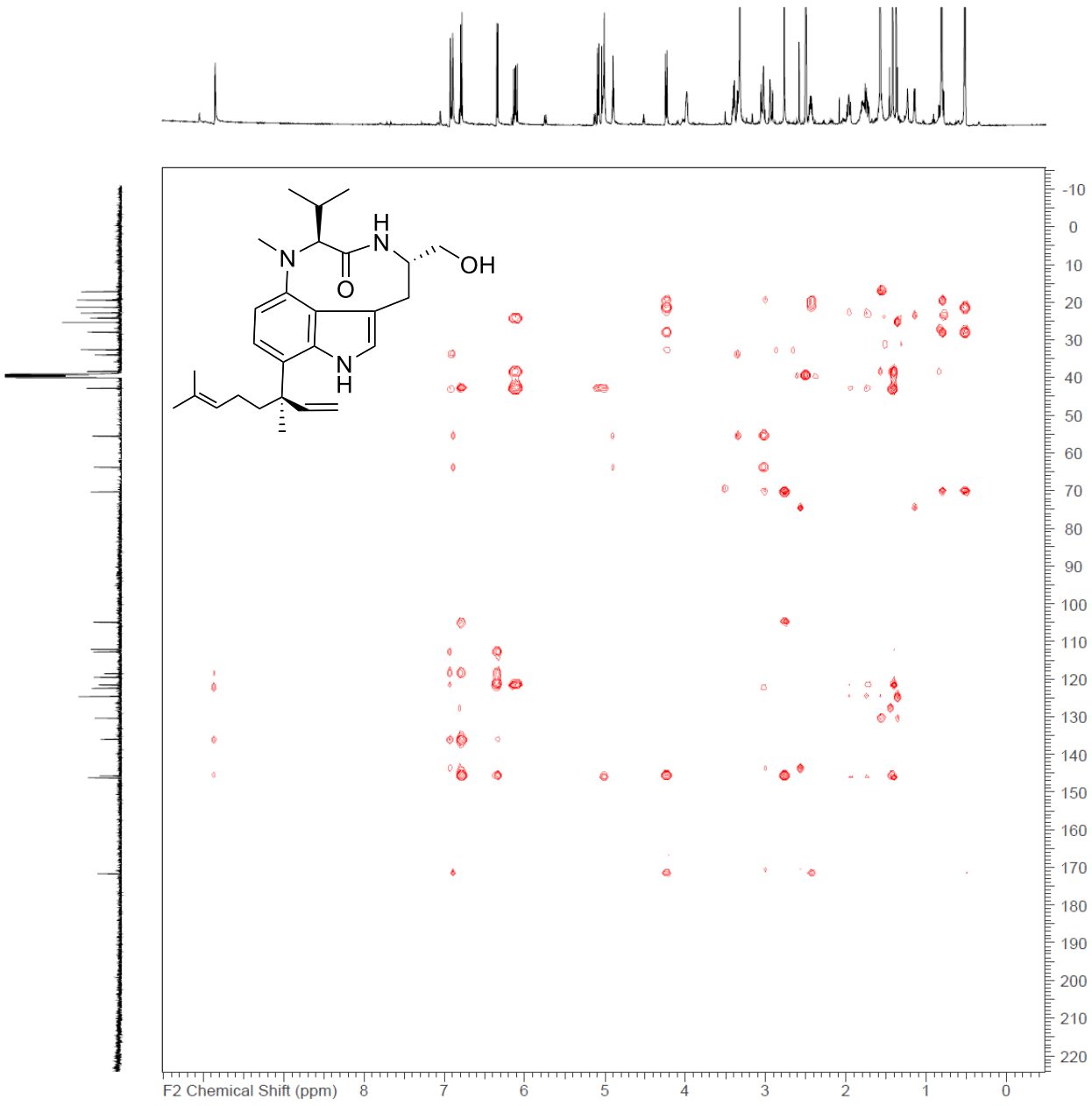

Figure 15. ^{1}H-^{13}C HMBC NMR spectra of **1** (teleocidin A-1). Spectra was collected in DMSO-*d*6.

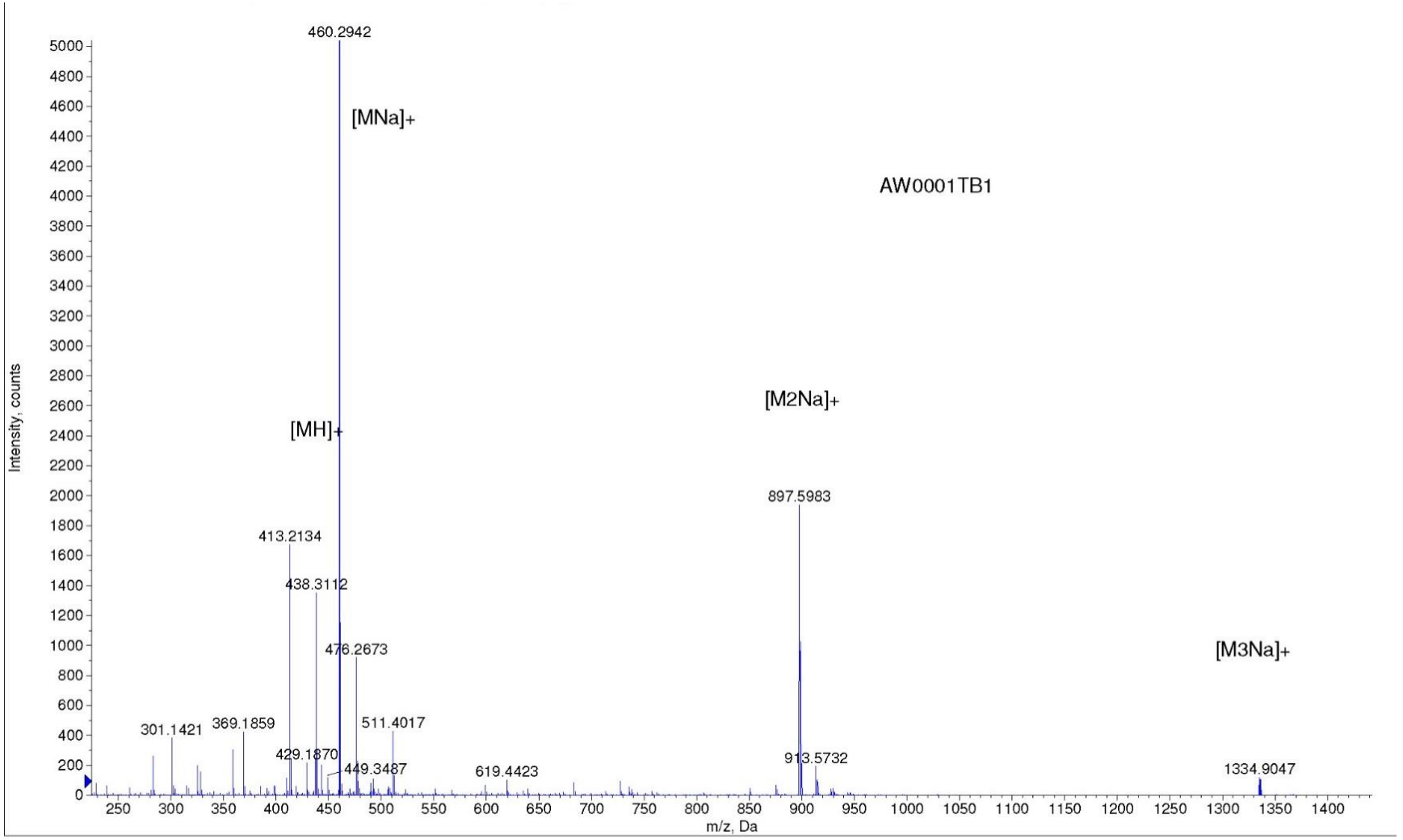

Figure 16. High resolution mass spectra of **1** (teleocidin A-1). A mass of 437.3112 Da was identified based on the protonated m/z signal of 438.3112 Da. Molecular formula determined as $C_{27}H_{39}N_3O_2$.

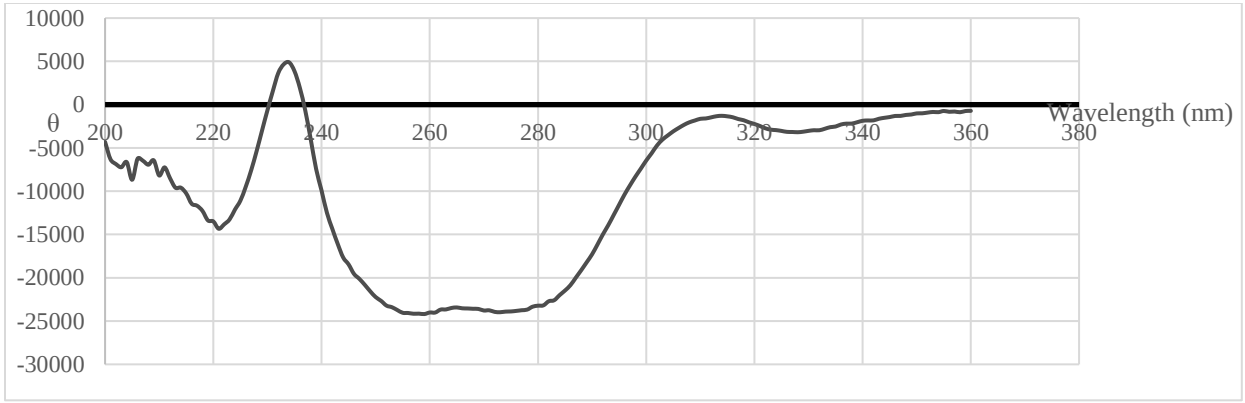

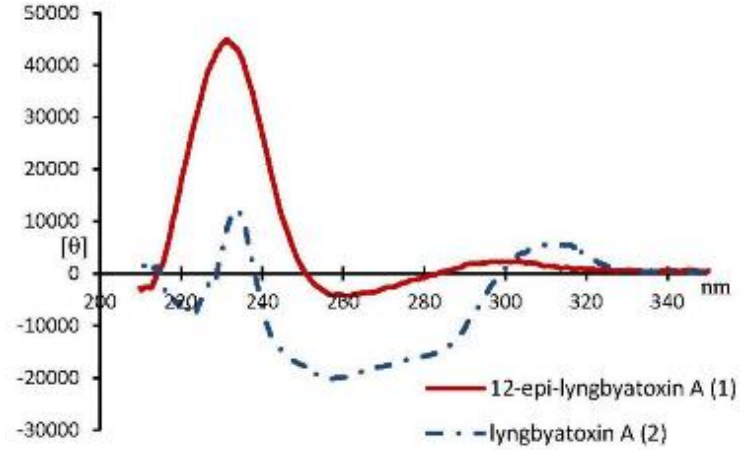

Figure 17. Circular Dichroism (CD) spectra of **1** (teleocidin A-1). Top: CD spectra data were obtained in MeOH as follows: $[\theta]_{230}$ = −655, $[\theta]_{234}$ = 4892, $[\theta]_{259}$ = −24189, $[\theta]_{314}$ = −1290, and $[\theta]_{328}$ = −3183. Optical rotation results indicated an overall degree of rotation of $[\alpha]_D^{20}$ = −35°. Bottom: CD spectra reported for lyngbyatoxin A (teleocidin A-1, **1**; blue dash line) and 12-epi-lyngbyatoxin A (red). Figure modified from Jiang, et. al. (2014).

NRPS/ladderane-arylpolyene, T3-PKS, and 2 unidentified domains. Clusters for kirromycin and candicidin that are separated for the same metabolite can be more appropriately joined together. Of the biosynthetic gene clusters identified, fewer than half are shared with those identified from an antiSMASH analysis of *Streptomyces* sp. TP-A0873. Inspection of the identified biosynthetic gene cluster for teleocidin-B production yielded the presence of one dimodular non-ribosomal peptide synthetase (*tleA*), one cytochrome P450 hydroxylase (*tleB*), a tryptophan dimethylallyl transferase (*tleC*), and an MbtH-like protein (Figure 18). However, the final enzyme necessary for terpene cyclization from **1** to **2** (*tleD*) was not identified in the downstream region of the gene cluster. The biosynthetic cluster assigned by antiSMASH to represent teleocidin B biosynthesis in Streptomyces sp. AVP053U2 also lacked the *tleD* gene needed for terpene cyclization. The genome sequenced was deposited into GenBank under the accession number LMTQ00000000.

D. Localization of Teleocidin Biosynthesis and Housekeeping Gene Regions

PCR amplification experiments were performed in DNA stocks taken from cultures of pure *Streptomyces* sp. AVP053U2 and from DNA isolated from *Styela clava* individuals collected from Avery Point, CT including the original voucher specimen that AVP053U2 was originally isolated from. These experiments aimed to evaluate the presence or absence of bacteria known for secondary metabolism of natural products with drug-like properties and specifically for teleocidin biosynthesis. Successful amplification of universal bacterial 16S rRNA genes and custom 16S rRNA gene segments were observed in DNA isolated from *Streptomyces* sp. AVP053U2, internal fluid collected from tunicate specimens, and environmental sea water samples (Figure 19). Internal fluid was isolated during dissection by draining and collecting all fluid material after excising the posterior end of the tunicate. Amplification of *S. clava* 18S rRNA housekeeping genes was successful in DNA isolated from *S. clava* tissue segments (Figure 19, Table 4). Teleocidin

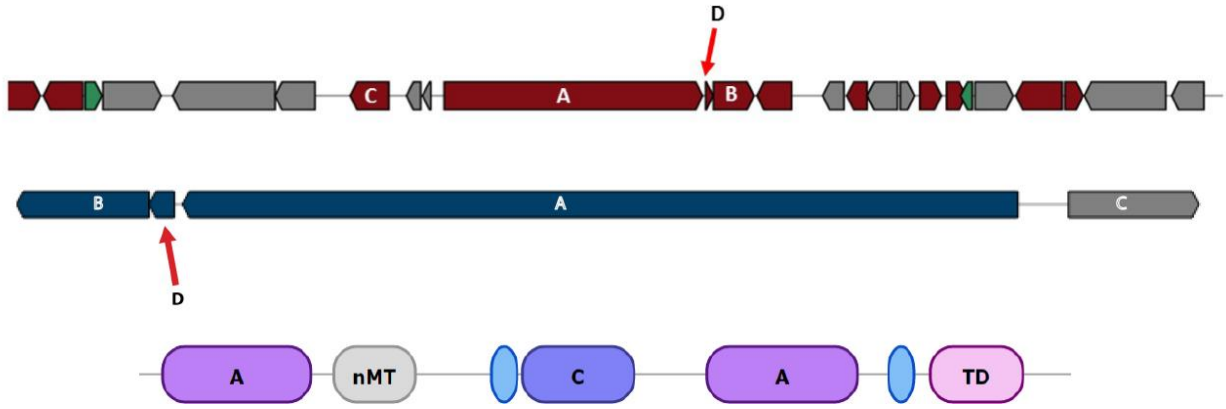

Figure 18. Comparison of biosynthetic gene clusters responsible for teleocidin. (Top) Biosynthetic gene cluster responsible for the production of teleocidin from the antiSMASH analysis of *Streptomyces* sp. AVP053U2. Figure represents genes based on the sequenced genome of AVP053U2. Putative biosynthetic genes are colored red, regulation-related genes are colored green, and other genes are colored gray. A: tleA – dimodular non-ribosomal peptide synthetase. B: tleB – cytochrome P450. C: tleC tryptophan dimethylallyl transferase. D: MbtH-like protein. (Middle) Database alignment of teleocidin biosynthetic gene cluster. A: tleA – dimodular non-ribosomal peptide synthetase. B: tleB – cytochrome P450. C: tleC tryptophan dimethylallyl transferase. D: MbtH-like protein. (Bottom) Domains identified for tleA gene segment. A: AMP-binding domain, nMT: n-methyl transferase, C: condensation domain, TD: threonine deaminase (Weber, et al., 2015)

biosynthesis amplification experiments were successful in DNA extracted from *Streptomyces* sp. AVP053U2 (Figure 20). Sequences of PCR products amplified with primers AVP16Sfor3/AVP16Srev3 and S.CLAVA18Sfor/S.CLAVA18Srev were submitted for BLAST analysis to ensure successful amplification of the intended sequence(s). Amplicon sequences of AVP053U2 16S rDNA aligned with organisms of the genus *Streptomyces* (BLAST E-value: 30,000; NCBI match Accession number: CM003601). In addition, as expected, *Styela clava* 18S amplicon sequences from tunicate tissues aligned with sequences for *Styela clava* 18S rDNA (BLAST E-value: 30,000; NCBI match Accession number: AH001758).

Primer BLAST analysis was used to identify other known organisms with similar DNA segments that could have been amplified during the reaction. Primer BLAST results for primers AVP16Sfor3/AVP16Srev3 indicate amplification of genomes that include, but are not limited to *S. anulatus, S. coelicolor, Streptomyces* sp. Root66D1, and *Streptomyces* sp. Root1310. AntiSMASH analysis of these additional genome assemblies highlight biosynthetic gene clusters for NRPS/PKS pathways that result in metabolites such as actinomycin, cyclohexamide, albaflavenone, cinerubin B, antimycin, and actinorhodin (Table 5). These biosynthetic gene clusters are also found in the genome assembled from *Streptomyces* sp. AVP053U2 (Table 6).

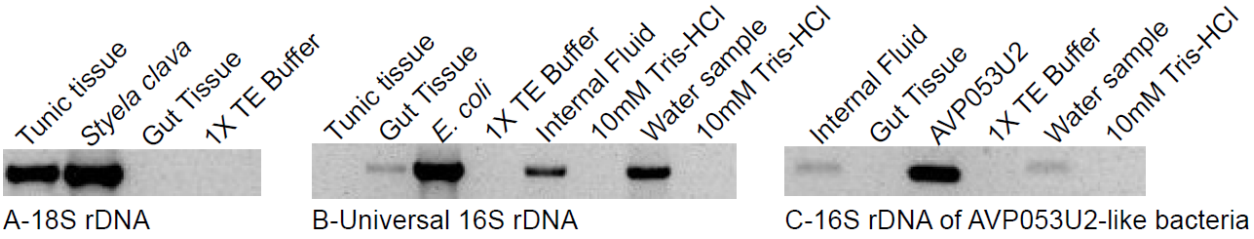

Figure 19. PCR amplification experiments of housekeeping genes in tunicate tissue. Amplicons analyzed via gel electrophoresis on a 1% agarose gel stained with ethidium bromide (0.5 µg/mL). Gel was run at a constant 80V for 1 hour. (A) *S. clava* 18S rDNA amplifications. *Styela clava* DNA used as positive control. 1X TE Buffer used as negative vehicle control for tunic and gut tissue DNA samples. (B) Universal 16S rDNA amplifications. E. coli DNA used as positive control. 1X TE Buffer used as a negative control for tunic and gut tissue DNA samples. 10mM Tris-HCl (Solution PW6 [MoBio Labs]) used as a negative control for both internal fluid and water sample DNA samples. Amplification experiments for internal fluid and for water sample DNA with universal 16S rDNA were performed separately and thus have two separate negative control runs. Samples with universal bacteria 16S rDNA were also examined for 16S rDNA of AVP053U2-like bacteria in C. (C) 16S rDNA region directed for *Streptomyces* sp. AVP053U2-like bacteria. DNA from *Streptomyces* sp. AVP053U2 used as a positive control. 1X TE Buffer used as a negative control for gut tissue DNA and 10mM Tris-HCl (Solution PW6 [MoBio Labs]) used as a negative control for internal fluid and water sample DNA.

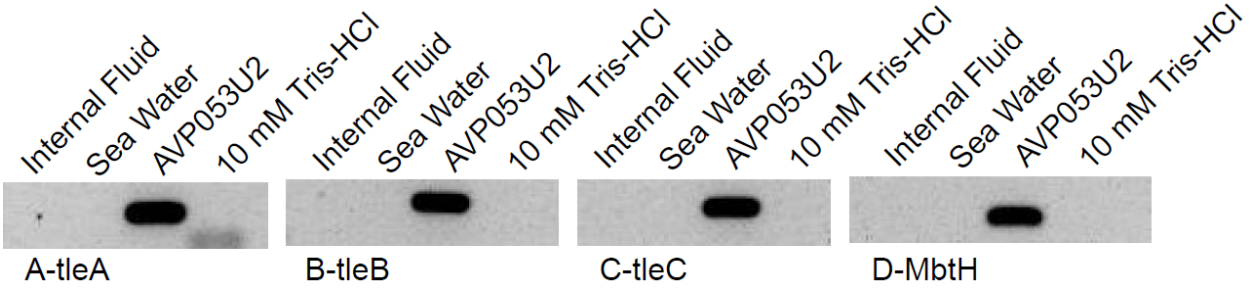

Figure 20. PCR amplification experiments of teleocidin biosynthesis genes. Experiments were conducted using DNA extracted from tunicate internal fluid and surface sea water. AVP053U2 used as a positive run control. 10 mM Tris-HCl (Solution PW6 [MoBio Labs]) used as a negative vehicle control. Conserved segments of each biosynthetic gene cluster were amplified. Entire gel included in Appendix B.

Table 4. PCR amplification results for presence or absence of 18S and 16S rRNA genes in extracted DNA. The experiments for identifying presence or absence of 18S rDNA and 16S rDNA regions are in genomic DNA samples isolated from tunicates, bacteria, and filtered sea water. “X” denotes successful amplification. “ – ” denotes unsuccessful amplification.

Sample	*S. clava* 18S rRNA	Universal 16S rRNA	*Streptomyces* specific 16S rRNA	Teleocidin Biosynthesis
Tunicate Tissue	X	-	-	-
Tunicate Fluid	-	X	X	-
AVP053U2	-	X	X	X
Sea Water	-	X	X	-
E. coli	-	X	-	-

Table 5. Closely related strains of *Streptomyces* identified via Primer BLAST and their associated biosynthetic gene clusters. Bacterial strains were investigated using antiSMASH for biosynthetic gene clusters.

Additional genomes identified	NCBI Accession Number	Featured sequences	Biosynthetic gene clusters identified
Streptomyces anulatus strain ATCC 11523	CM003601	16S rRNA	Actinomycin, cyclohexamide, oxazolomycin, griseobactin, coelichelin, incednine, herboxidiene, streptolydigin, borrelidin, steffimycin, ectoine, desferrioxamine B, tetronasin, skyllamycin, enduracidin, rabelomycin, landomycin, 2-methylisoborneol, nonactin, hopene, legonaridin, actinomycin, melanin, daptomycin
Streptomyces sp. Root66D1	LMHG01000001	16S rRNA	Cinerubin B, istamycin, xantholipin, venezuelin, quartomicin, platencin, friulimicin, desferrioxamine B, hopene, ectoine, versipelostatin, 2-methylisoborneol
Streptomyces sp. Root1310	LMEQ01000001	16S rRNA	Albaflavenone, antimycin, ectoine, lactonamycin, desferrioxamine B, meridamycin, hopene, akaeolide, furaquinocin A, albaflavenone, alnumycin, indanomycin, endophenazine, caprazamycin, laspartamycin, rifamycin, nigericin, labyrinthopeptin, pyridomycin, legonaridin, mitomyicn, melanin, phoslactomycin, scabichelin, herbimycin
Streptomyces coelicolor	NC_003888	16S rRNA	Leinamycin, isorenieratene, sanglifehrin A, coelichelin, informatpeptin, herboxidiene, ectoine, lactonamycin, desferrioxamine B, albaflavenone, actinorhodin, spore pigment, undecylprodigiosin, enduracidin, coelimycin, nogalamycin, hopene, arsenopolyketides, ravidomycin, coelibactin

IV. Discussion

A. Screening of Tunicate-Associated Bacterial Extracts

The assay described previously represents an evaluation of cytotoxic T-lymphocyte (CTL) lytic granule exocytosis and suppression as a result of stimulation with small molecules. Stimulation with addition of TG and PMA help guide the evaluation of specific mechanism of action for enhancement of lytic granule exocytosis. Investigation of secondary metabolites have often led to the identification of novel and interesting small molecule therapeutics (Li and Vederas, 2009). A library of unknown bacterial secondary metabolite extracts was successfully screened, identifying a potent PKC enhancing molecule whose mechanism of action was further investigated. In preliminary testing, higher testing concentrations of compound E1 yielded low levels of granule exocytosis, leading us to believe that E1 augmented immune system response by limiting PKC activation. However, previous reports of cell degradation as a result of PKC augmenting compounds indicate that in response to PKC activators, PKC over-activation and prolonged exposure have been demonstrated to lead to ubiquitination and degradation (Lu, et al., 1998). Our initial data suggests that an increase in concentration of E1 leads to cell death as a result of PKC over-activation and results in an apparent inhibitory effect. Repeat experiments indicated that at lower concentrations E1 was responsible for PKC activation independent of intracellular calcium concentration (Figure 10). As a result, E1 is an unlikely candidate for treatment of immune disorders because of its over-activation potential.

Elucidation of the pure compound structure involved thorough analysis of NMR, HRMS, optical rotation, and CD spectra. Two-dimensional NMR spectra were used to assign proton and carbon nuclei associations through space and across multiple bond correlations. Optical rotation and CD experiments are used to analyze molecular three-dimensional orientation, and confirmed

its conformation as teleocidin A-1 (**1**). A mass of 437.3112 Da was determined from the protonated *m/z* of 438.3112 Da. The chemical formula was consistent with ten degrees of unsaturation attributed to three ring structures, and seven pi bonds throughout the molecule. Data collected through NMR and polarimetry experiments coupled with the mass spectra helped to identify the overall structure as known PKC-activating metabolite teleocidin A-1. Three chiral carbons in the overall structure allow for a total of eight possible configurations and enantiomers. Optical rotation and CD data were able to identify the three-dimensional structure as the previously isolated metabolite **1** (Figure 17). Comparison of the remaining NMR data was in close agreement with to reported literature data for **1**.

Comparison of the dose-response measurements for PKC activation between PMA and **1** (Figure 7D) led us to investigate the specific mechanism of action of **1** in complex with PKC activation. Previous research for secondary activation of PKC with phorbol esters such as PMA indicate binding events within the C1B domain of PKC isoforms (Zhang, et al., 1995). In fact, docking experiments comparing the pharmacophore model of the indolactam-V moiety that comprises the majority of the **1** scaffold and PMA binding within the C1B domain of PKC highlight three of the four hydrogen binding events shared between the two ligands (Wang, et al., 1999). Flexibility of the indolactam-V moiety has been shown to have two major conformations: the *cis*-twist conformation and *trans*-sofa conformation (Figure 21). Evaluation of both conformations in the C1B domain binding site of PKC identified the cis-twist conformation of indolactacm-V as the dominant and most likely conformation for PKC activation (Wang, et al., 1999). X-Ray crystal data for C1B binding to the indolactam-V moiety highlights hydrogen bonding between hydroxyl and carbonyl functional groups within the indolactam-V scaffold, and the Thr12 and Gly23 amido groups, respectively (Figure 22) (Wang, et al., 1999). Three chiral

carbon centers allow for eight distinct configurations, however only teleocidin A-1 (Takashima and Sakai, 1960), 2-oxo-3(R)-hydroxy-lyngbyatoxin A and 2-oxo-3(R)-hydroxy-13-N-desmethyl-lyngbyatoxin A (Jiang, et al., 2014), and 9,12-epi lyngbyatoxin A (Awakawa, et al., 2014) have ever been observed in nature. Comparison of collected data to previously reported optical rotation and CD data confirm the conformation shown above (Figure 17).

Compared to screening synthetic compound collections, screening of natural product extract libraries presents several difficulties in the search for novel compounds with biomedically relevant activities (Li and Vederas, 2009). Extracts are complex mixtures of compounds that often range in polarity and solubility. Active natural product compounds may be present in only minute quantities, and their activity may be overshadowed by other bioactive components or interfering nuisance compounds within the mixture. Crude extracts often contain pigmented compounds and may also contain autofluorescent metabolites. In addition, compounds may be less soluble when isolated and/or be unstable when not in the extract matrix. Furthermore, Zhao, et. al. (2016) demonstrated that compounds that affect lytic granule exocytosis would affect immune functions that involve lytic granule exocytosis, and on this basis might be expected to modulate antiviral and antitumor immunity. It is likely that many of the compounds identified as active in a screen based on lytic granule exocytosis, such as **1** or its derivatives would also affect the activity of other immune cells. As a result, this screening strategy can be applied to other cell types that respond to stimuli presented on a solid phase. The data presented by Zhao, et al. (2016) indicates that while some cells may only respond to soluble stimuli or may not produce optical scatter properties that allow their identification via flow cytometry, the assay is suitable for screening natural product extract libraries as part of an activity-guided fractionation scheme, and for repurposing previously identified bioactive molecules.

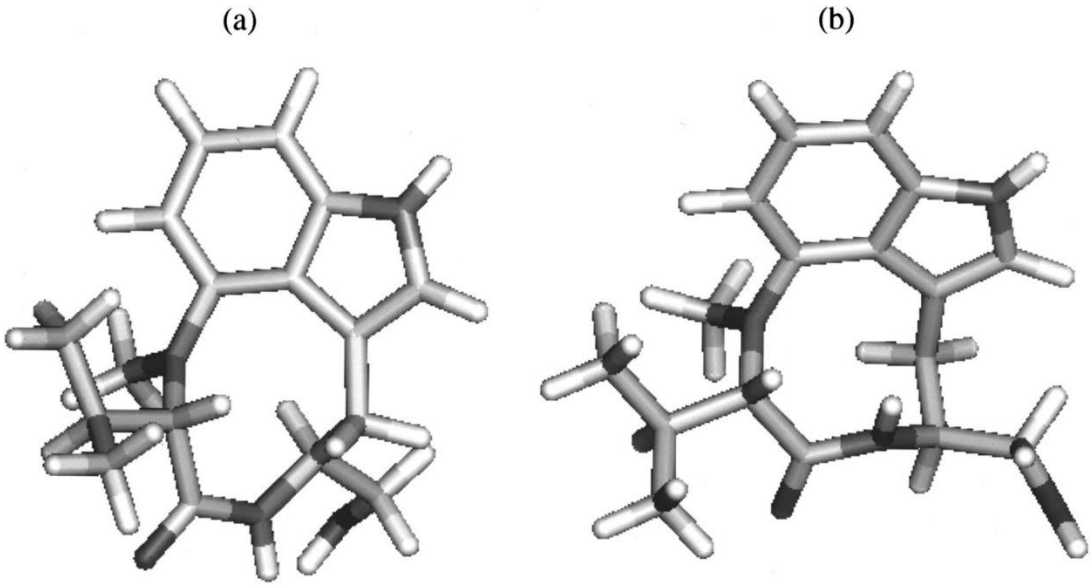

Figure 21. (A) *Cis*-twist and (B) *trans*-sofa conformations of indolactam-V during binding with PKC. The indolactam-V scaffold is responsible for extensive binding events in the C1B binding domain of PKC by teleocidin A-1 (**1**). The *cis*-twist conformation has been demonstrated as the dominant conformation for binding within the C1B domain of PKC (Wang, et al., 1999).

B. Bacterial Genome Investigation

Our investigations of **1** as a promoter of CTL granule exocytosis led us to explore the bacteria responsible for secondary metabolite biosynthetic gene clusters and to evaluate its phylogeny. Preliminary BLAST comparisons of the 16S rRNA gene sequence identified our new isolate as a member of the genus *Streptomyces*. Using the ORFcor pipeline for phylogenetic analysis (Klassen and Currie, 2013) allowed us to identify the closest relative of our *Streptomyces* bacteria as a previously identified *Streptomyces* bacterium isolated from the deep ocean in the western Pacific Ocean near Japan known as *Streptomyces* sp. TP-A0873 (Figure 23 and Appendix B) (Komaki, et al., 2015). Both genomes, when analyzed using antiSMASH were shown to contain the biosynthetic gene cluster responsible for production of teleocidin B, a derivative of **1**. The biosynthesis of teleocidin B includes the same three domains necessary for production of **1** with the addition of a fourth methyltransferase enzyme necessary for terpene cyclization known as *tleD*. Teleocidin B biosynthesis was derived from the genome of *Streptomyces* bacteria (Awakawa, et al., 2014). As mentioned earlier, **1** was later reisolated from the cyanobacterium *Moorea producens* (formerly *Lyngbya majuscula*) and named lyngbyatoxin A (Cardellina II, et. al. 1979). After rediscovery, the biosynthetic pathways associated with lyngbyatoxin A (teleocidin A-1, **1**) were evaluated in cyanobacteria and the relevant PKS/NRPS enzymes were identified (Edwards and Gerwick, 2004). The antiSMASH results categorized biosynthetic gene clusters from our assembled genome with that of other genome sequences deposited for *Streptomyces* bacteria. Because all of the necessary gene sequences required for the biosynthesis of **1** are included in teleocidin B, it is likely that antiSMASH grouped the gene clusters identified for **1** with the closest partial biosynthetic gene cluster derived from other *Streptomyces* bacteria, namely teleocidin B.

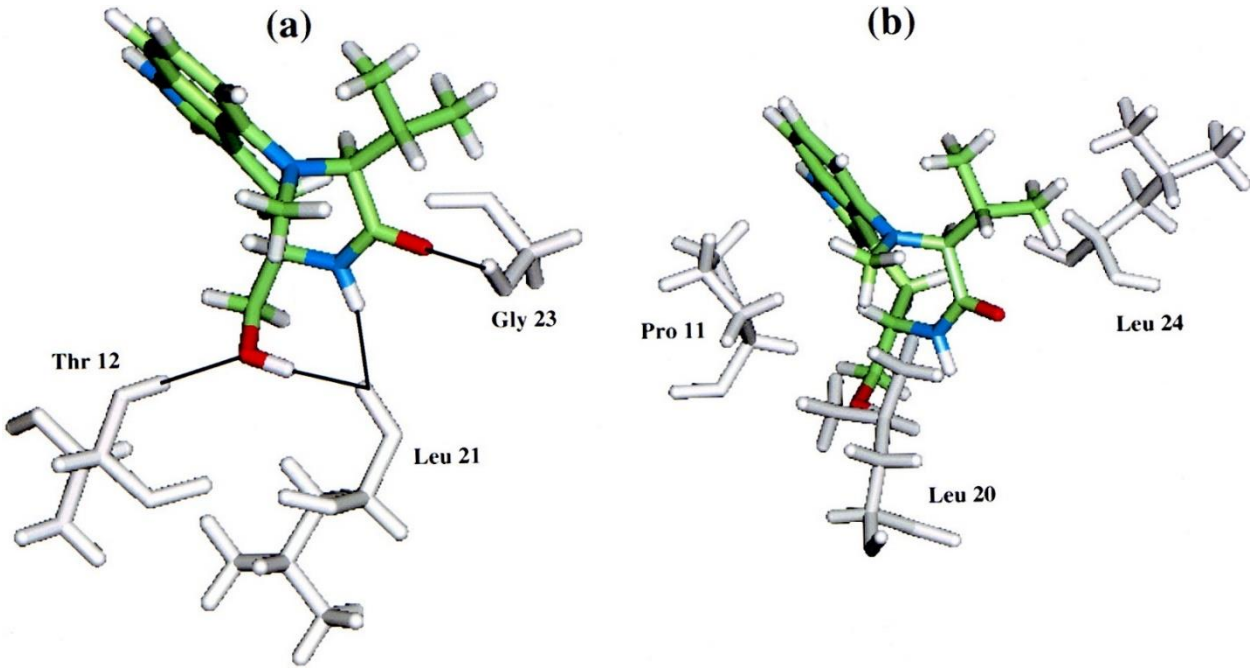

Figure 22. X-Ray crystal data of (a) *cis*-twist conformation and (b) *trans*-sofa conformation of the indolactam-V during binding with PKC. The indolactam-V structure (green) highlights stronger hydrogen bonding between hydroxyl and carbonyl functional groups within the cis-twist indolactam-V scaffold, and the Thr12 and Gly23 amido groups, respectively residues among the C1B domain on PKC (CITE). The Leu21 amido group is also implicated in weaker hydrogen bonding events with the hydroxyl group and amido group within indolactam-V (Wang, et al., 1999).

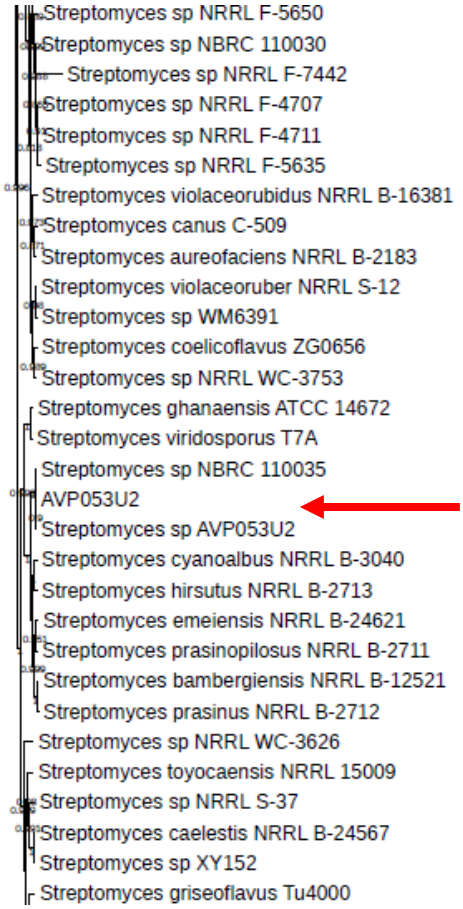

Figure 23. Gene phylogeny tree of Streptomyces bacteria in NCBI library. This figure represents a portion of the phylogenetic tree created using fasttree (Price, 2009) (Price, 2010) from a set of conserved homologs using the ORFcor pipeline (Klassen and Currie, 2013) that were automated using MUSCLE (Edgar, 2004) and compares our draft genome with the entire NCBI library of *Streptomyces* bacteria (Jonathan Klassen, UConn Dept. of Molecular and Cellular Biology). *Streptomyces* sp. TP-A0873 was isolated from the deep Pacific off the Japanese coast, while *Streptomyces* sp. AVP053U2 was isolated from shallow surface water within Long Island Sound. The differences in genome sequence can be seen in the differences in biosynthetic gene clusters as evaluated by antiSMASH (Weber, et al., 2015). While both genomes have high overall sequence homology, fewer than half of the biosynthetic gene clusters identified share greater than 75% nucleotide sequence homology. The full phylogenetic tree is in Appendix B.

In addition to production of **1**, other medically relevant biosynthetic gene clusters were identified within the genome of our bacteria. *Streptomyces* bacteria have historically been responsible for the production of interesting bioactive metabolites (Watve, et al., 2001). Investigation of identified biosynthetic gene clusters identified several biologically relevant secondary metabolite gene clusters including the known antibiotic albaflavenone (Table 6). Interestingly, investigation of the closest known relative of *Streptomyces* sp. AVP053U2, *Streptomyces* sp. TP-A0873, identified many of the same biosynthetic gene clusters present within the whole genome assembly. However, of the identified gene clusters shared between the two genomes, fewer than half of them shared greater than 75% sequence identity (Table 6). These differences in gene cluster sequence were likely the cause for the 0.3% difference in the overall phylogenetic separation, leading to a previously unidentified strain of *Streptomyces*.

C. Localization of Bacteria in Tunicate Tissue

The activity associated with granule exocytosis and PKC activation for **1** led us to question where sequestration of the bacteria took place within the tunicate in order to examine proximity of the bacteria to various tunicate metabolic pathways. Previous research has identified various bacterial associations for colonial tunicates within specific tissues (Riesenfeld, et al., 2008), but few studies have been performed investigating the location of bacterial symbionts amongst solitary tunicates such as *Styela clava*.

However, the model solitary ascidian *Ciona intestinalis* has been demonstrated to harbor bacterial communities at various life stages within the gut region (Dishaw, et al., 2014) and within the tunic tissue (Blasiak, et al., 2014). Although, the authors expressed surprise at the dense population of intratunic bacteria amongst the *Ciona* specimens. Associations with symbiotic

Table 6. AntiSMASH analysis of the genome assembled for *Streptomyces* sp. AVP053U2 and *Streptomyces* sp. TP-A0873 (Weber, et al., 2015). Relevant biosynthetic gene clusters were noted and the percent amino acid similarity for the aligned segment of each biosynthetic gene cluster is listed for each gene cluster. Cluster number denotes position in genome sequence. Percent similarity refers to similarity of examined genome sequences to database biosynthetic gene cluster data. Gene clusters without percent similarity rating were only identified to the type level. Genome for *Streptomyces* sp. AVP053U2 deposited in GenBank under the accession number: LMTQ00000000. Genome for *Streptomyces* sp. TP-A0873 accessed from GenBank using the accession number: BBNN00000000 (Komaki, et al., 2015).

Streptomyces sp. AVP053U2

Cluster Number	Type	Most Similar Known Cluster	Percent Similarity
1	Terpene-T2pks	Spore Pigment	75
2	Indole-NRPS	Teleocidin B	100
3	Melanin	-	-
4	other	Calcimycin	10
5	Siderophore	Desferrioxamine B	66
6	Terpene	-	-
7	Siderophore	-	-
8	T1pks	Borrelidin	46
9	Terpene	Albaflavenone	100
10	Lantipeptide-NRPS	Streptomycin	12
11	Butyrolactone-T1pks	Tetronasin	3
12	NRPS	Zorbamycin	4
13	NRPS-T1pks	Antimycin	100
14	Butyrolactone	γ-Butyrolactone	100
15	Nucleoside	Toyocamycin	40

Streptomyces sp. TP-A0873

Cluster Number	Type	Most Similar Known Cluster	Percent Similarity
1	Butyrolactone	γ-Butyrolactone	100
2	Transatpks	Leinamycin	7
3	NRPS	Akaeolide	12
4	otherks-T2pks	Cosmomycin D	62
5	Bacteriocin	-	-
6	Terpene	-	-
7	Siderophore	-	-
8	Ectoine	Ectoine	75
9	NRPS-T1pks	Antimycin	100
10	NRPS-T1pks	Zorbamycin	4
11	NRPS-Terpene	Albaflavenone	100
12	Lantipeptide-NRPS	Streptomycin	7
13	Indole-NRPS	Teleocidin B	100
14	other	Kirromycin	27
0	Melanin	Melanin	40

16	Terpene	Isorenieratene	100
17	Ectoine	Ectoine	100
18	NRPS	Chalcomycin	4
19	T1pks	-	-
20	Terpene	-	-
21	Bacteriocin	Sisomicin	5
22	NRPS-Ladderane-Arylpolyene	Skyllamycin	18
23	Terpene	Hopene	76
24	T1pks	Candicidin	80
25	NRPS	Candicidin	38
26	T3pks-NRPS	UK-68,597	17
27	NRPS-T1pks-Transatpks	Kirromycin	13
28	NRPS-T1pks	-	-
29	Amglyccycl-NRPS	Arsenopolyketides	12
30	Terpene	-	-
31	NRPS	Enduracidin	12
32	Lantipeptide	-	-
33	Lantipeptide	-	-
34	other	Kirromycin	23
35	NRPS	-	-
36	T1pks	-	-
37	T1pks	-	-
38	NRPS	-	-
39	T1pks	-	-
40	NRPS	-	-
41	Lantipeptide	-	-
42	NRPS	-	-
43	NRPS	WS9326	10
44	NRPS	-	-
45	T1pks	-	-
46	NRPS	-	-

16	other	Chloramphenicol	23
17	Siderophore	Desferrioxamine B	66
18	Terpene	-	-
19	Terpene	Hopene	76
20	Terpene	Isorenieratene	100
21	Nucleoside	Toyocamycin	40
22	Terpene-T2pks	Spore-Pigment	83
23	Arylpolyene	Laspartomycin	9
24	NRPS	Candicidin	38
25	T1pks	Candicidin	85
26	NRPS	Chalcomycin	4
27	T1pks	Nystatin	18
28	Butyrolactone-T1pks	Tetronasin	3
29	Terpene	-	-
30	NRPS	Pristinamycin	5
31	T1pks	-	-
32	Lantipeptide	-	-
33	Ladderane-Arylpolyene	Colabomycin	9
34	T1pks	Apoptolidin	15
35	T1pks	-	-
36	T1pks	-	-
37	NRPS	Tirandamycin	33
38	T1pks	-	-

Prochloron cyanobacteria and host didemnid tunicates such as *Lissoclinum patella* have been extensively studied, yet fewer associations have been established for symbiotic heterotrophic bacteria and solitary tunicates (Lin, et al., 2016). In addition, bacterial associations with invasive tunicate species are often highly variable. It is thought that the associations of bacteria to host tunicates can aid in acclimation to new environments by establishing relationships with new locally-sourced bacteria (Erwin, et al., 2013). Because of the lack of bacterial genes amplified from tunicate tissue DNA extracts, the data presented here suggests that solitary tunicates such as *Styela clava* are less dependent on bacterial populations than other, more densely populated tunicate colonies, and thus harbor less bacteria within their tissue.

Experiments were designed to investigate the presence of bacteria within various tissue DNA samples extracted from the tunicate specimens. Bacterial presence was verified in DNA samples extracted from the tunicate gut using PCR to amplify universal 16S rRNA regions of DNA. Surprisingly, however, the same region of DNA in samples taken from tunic tissue of *Styela clava* specimens did not indicate the presence of 16S rRNA. This could be a result of two scenarios: 1) bacterial DNA was not present intratunically or 2) it is possible that there was degradation of bacterial DNA as a result of the freeze-thaw cycles during DNA extraction.

While it is often seen that undiscovered bacterial isolates can originate from tunic-derived bacterial cultures, it is not clear whether the cultures are present from intratunic bacteria or surface dwelling transient organisms. Interestingly, DNA from internal fluid contained regions of the *Streptomyces* 16S rRNA gene (Figure 19). This data implies that bacteria are not only housed within the tissue belonging to the tunicate, but are transported via the circulatory system, likely as a byproduct of the filter feeding mechanism. This was perhaps the most significant result, as it identified the presence of these biomedically relevant strains of bacteria within the environment

of the tunicate specimens. Moreover, upon examination of the DNA extracted from the surrounding sea water, the same universal bacterial housekeeping genes and specialized *Streptomyces*-linked genes were identified (Figure 19). As mentioned earlier, genomes identified from the *Streptomyces*-linked amplicons have demonstrated potential for production of antibiotic secondary metabolites. As a result, using the assembled genome sequence from *Streptomyces* sp. AVP053U2 can help to identify other bacterial strains with the potential for medically relevant secondary metabolites in addition to our own new strain of *Streptomyces*.

After identifying the presence of bacteria within the select groups of tunicate tissue DNA and surrounding sea water, specific teleocidin biosynthesis gene sequences were investigated in the same samples of DNA. The results indicated that although select regions of teleocidin biosynthesis genes were able to amplify in DNA extracted from isolated bacteria, the same regions did not amplify in DNA taken from the tunicate internal fluid or surrounding sea water (Figure 20). The inability to identify teleocidin biosynthesis genes may be attributed to two possible scenarios: 1) sequences for teleocidin biosynthesis are diluted within the mixture of extracted DNA taken from tunicate tissues to amplify or 2) bacteria that are present within the tunicate gut, internal fluid, or surrounding sea water do not contain the biosynthetic gene clusters for teleocidin biosynthesis.

V. Conclusions

This research was initiated to identify novel CTL augmenting metabolites extracted from tunicate-associated bacteria. The assay was designed for screening and identifying small molecule metabolites that enhance CTL granule exocytosis via PKC activation. From an extract of *Streptomyces* sp. AVP053U2 isolated from the tunicate *Styela clava*, we identified a potent PKC activator, teleocidin A-1 (**1**). Moreover, we were able to detect that activation of PKC by **1** was independent of intracellular calcium concentration.

Following assay validation and chemical structure elucidation, the genome of the previously unidentified bacteria was sequenced and examined for the potential for production of other biologically relevant metabolites. This data allowed for exploration of other *Streptomyces* bacterial symbionts of *Styela clava*. When examined for secondary metabolite potential, other *Streptomyces* bacteria were shown to contain similar biosynthetic capabilities as the newly identified *Streptomyces* sp. AVP053U2. Further investigation using alternate techniques may allow for increased identification of associated bacteria in order to detect bacterial presence, and may localize the bacteria to other tissue segments more definitively. However, this data suggests that the majority of the bacteria that associate with *Styela clava* are localized to the internal segments of the body as opposed to the external tunic membranes.

VI. **Appendix A**

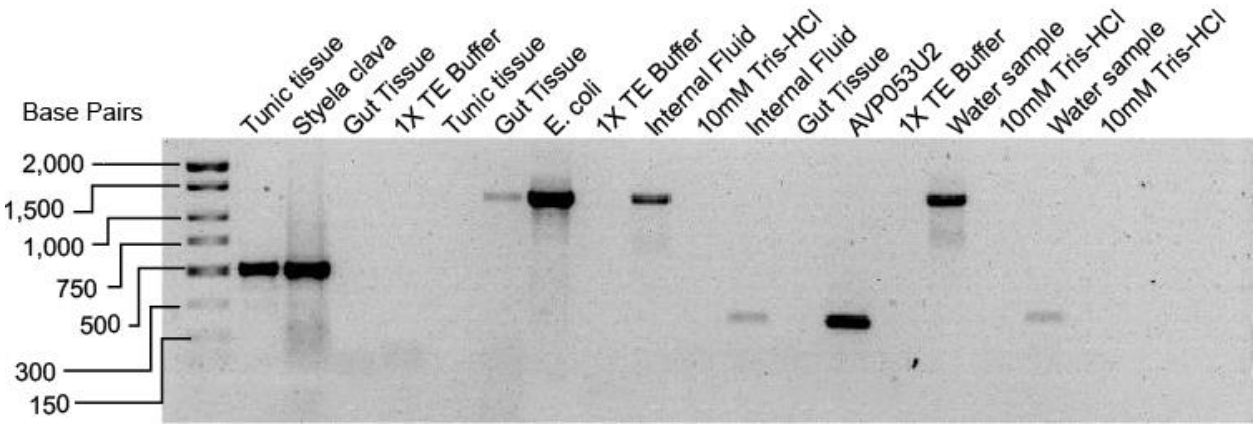

Appendix A. Summary of PCR amplification experiments for 18S and 16S housekeeping genes. Lanes 2-5 represent amplification of S. clava 18S rDNA. *Styela clava* DNA used as positive control. 1X TE Buffer used as negative vehicle control for tunic and gut tissue DNA samples. Lanes 6-11 and 16-17 represent amplification of universal 16S rDNA. *E. coli* DNA used as positive control. 1X TE Buffer used as a negative control for tunic and gut tissue DNA samples. 10mM Tris-HCl (Solution PW6 [MoBio Labs]) used as a negative control for both internal fluid and water sample DNA samples. Amplification experiments for internal fluid and for water sample DNA with universal 16S rDNA were performed separately and thus have two separate negative control runs. Samples that were indicated for universal bacteria 16S rDNA were also examined for 16S rDNA of AVP053U2-like bacteria. Lanes 12-15 and 18-19 represent amplification of selected region of *Streptomyces* sp. AVP053U2 16S rDNA. DNA from *Streptomyces* sp. AVP053U2 used as a positive control. 1X TE Buffer used as a negative control for gut tissue DNA and 10mM Tris-HCl (Solution PW6 [MoBio Labs]) used as a negative control for internal fluid and water sample DNA.

VII. **Appendix B**

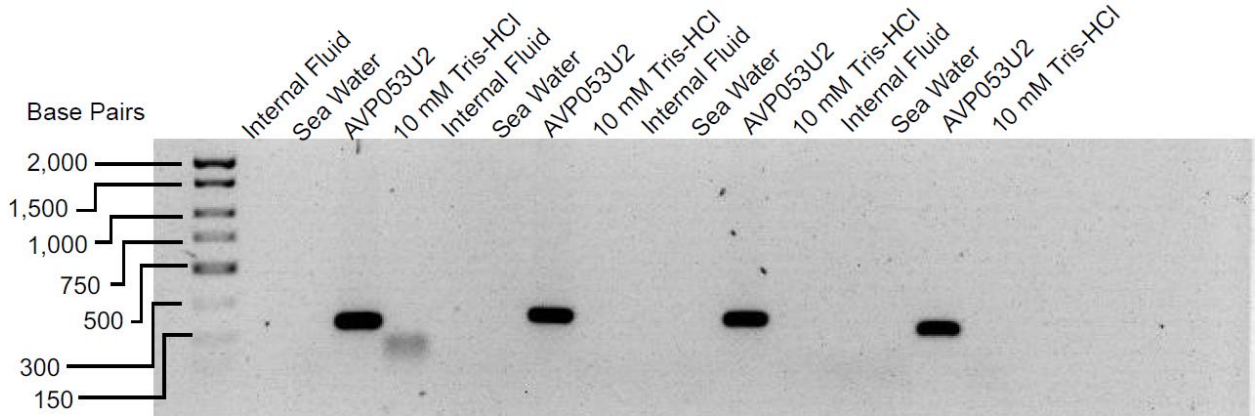

Appendix B. Gel electrophoresis of teleocidin biosynthesis gene segments in DNA from internal fluid and surface sea water. DNA from *Streptomyces* sp. AVP053U2 used as a positive control. 10 mM Tris-HCl (Solution PW6 [MoBio Labs]) used as a negative vehicle control. Lanes 2-5 represent amplification of tleA gene fragment. Lanes 6-9 represent amplifications of tleB gene fragments. Lanes 10-13 represent amplification of tleC gene fragment. Lanes 14-17 represent amplification of MbtH-like gene. The band in lane 4 represents primer dimerization during the PCR reaction.

References

2016. *Google Maps.* Available at: https://www.google.com/maps/place/41%C2%B018'58.5%22N+72%C2%B003'38.8%22W/@41.3159742,-72.0698386,15z/data=!4m5!3m4!1s0x0:0x0!8m2!3d41.31625!4d-72.0607833

Arcoleo, J. P. and Weinstein, I. B. Activation of protein kinase C by tumor promoting phorbol esters, teleocidin and aplysiatoxin in the absence of added calcium. *Carcinogenesis,* **1985**, *6*, 213-217.

Awakawa, T., Zhang. L., Wakimoto, T., Hoshino, S., Mori, T., Ito, T., Ishikawa, J., and Tanner, M. E., Abe, I. A methlytransferase initiates terpene cyclization in teleocidin B biosynthesis. *Journal of the American Chemical Society,* **2014**, *136*, 9910-9913.

Beckers, B., De Beeck, M. O., Thijs, S., Truyens, S., Weyens, N., Boerjan, W., Vangronsveld, J. Performance of 16S rDNA primer pairs in the study of rhizosphere and endosphere bacterial microbiomes in metabarcoding studies. *Frontiers in Microbiology*, **2016**, *7*, 650.

Blasiak, L. C., Zinder, S. H., Buckley, D. H. and Hill, R. T. Bacterial diversity associated with the tunic of the model chordate *Ciona intestinalis*. *ISME Journal,* **2014**, *8*, 309-320.

Cardellina II, J. H., Marner, F.-J. and Moore, R. E. Seaweed dermatitis: structure of lyngbyatoxin a. *Science,* **1979**, *204*, 193-195.

Coil, D., Jospin, G. and Darling, A. E. A5-miseq: an updated pipeline to assemble microbial genomes from Illumina MiSeq data. *Bioinformatics,* **2015**, *31*, 587-589.

Davies-Coleman, M. T. and Veale, C. G. L. Recent advances in drug discovery from south african marine invertebrates. *Marine Drugs,* **2015**, *13*, 6366-6383.

De Tomaso, A. W. Sea squirts and immune tolerance. *Disease Models and Mechanisms,* **2009**, *2*, 440-445.

deMayo, J. A., Maas, K. R., Klassen, J. L. and Balunas, M. J. A new teleocidin-producing *Streptomyces* bacteria isolated from tunicate host *Styela clava*. *Genome Announcements,* **2016**, *4*, e00874-16

Dishaw, L. J., Flores-Torres, J., Lax, S., Gemayel, K., Leigh, B., Melillo, D., Mueller, M. G., Natale, L., Zucchetti, I., De Santis, R., Pinto, M. R., Litman, G. W., and Gilbert, J. A. The gut of geographically disparate *Ciona intestinalis* harbors a core microbiota. *PLoS ONE,* **2014**, *9*, e93386.

Edgar, R. C., MUSCLE: multiple sequence alignment with high accuracy and high throughput. *Nucleic Acids Research,* **2004**, *32*, 1792-1797.

Edwards, D. J. and Gerwick, W. H. Lyngbyatoxin biosynthesis: Sequence of biosynthetic gene cluster and identification of a novel aromatic prenyltransferase. *Journal of the American Chemical Society,* **2004**, *126*, 11432-11433.

Erwin, P. M., Pineda, M. C., Webster, N., Turon, X., and Lopez-Legentil, S. Small core communities and high variability in bacteria associated with the introduced ascidian *Styela plicata*. *Symbiosis,* **2013**, *59*, 35-46.

Frank, J. A., Reich, C. I., Shobha, S., Weisbaum, J. S., Wilson, B. A., Olsen, G. J. Critical evaluation of two primers commonly used for amplification of bacterial 16S rRNA genes. *Applied and Environmental Microbiology*, **2008**, *74*, 2461-2470.

Fuke, M. T. and Numakunai, T. Allogeneic cellular reactions between intra-specific types of a solitary ascidian, *Halocynthia roretzi*. *Developmental and Comparative Immunology,* **1982**, *6*, 253-261.

Gasparini, F. Caicci, F., Rigon, F., Zaniolo, G., and Manni, L. Testing an unusual in vivo vessel network model: a method to study angiogenesis in the colonial tunicate *Botryllus schlosseri*. *Scientific Reports,* **2014**, *4.*

Gil-Turnes, M. S., Hay, M. E. and Fenical, W. Symbiotic marine bacteria chemically defend crustacean embryos from a pathogenic fungus. *Science,* **1989**, *246*, 116-118.

Glasel, J. A. Validity of nucleic acid purities monitored by 260nm/280nm absorbance ratios. *Biotechniques: The International Journal of Life Science Methods,* **1995**, *18*, 62-63.

Goris, J. Konstantinidis, K. T., Klappenbach, J. A., Coenye, T., Vandamme, P., and Tiedje, J. M. DNA-DNA hybridization values and their relationship to whole-genome sequence similarities. *International Journal of Systematic and Evolutionary Microbiology,* **2007**, *57*, 81-91.

Ireland, C., and Scheuer, P. J. Ulicyclamide and ulithiacyclamide, 2 new small peptides from a marine tunicate. *Journal of the American Chemical Society*, **1980**, *102*, 5688-5691.

Jiang, W., Zhou, W., Uchida, H., Kikumori, M., Irie, K., Watanabe, R., Suzuki, T., Sakamoto, B., Kamio, M., and Nagai, H. A new lyngbyatoxin from the hawaiian cyanobacterium *Moorea producens*. *Marine Drugs,* **2014**, *12*, 2748-2759.

Klassen, J. L. and Currie, C. R. Identifying and accommodating ORF prediction inconsistencies for phylogenetic analysis. *PLoS ONE,* **2013**, *8*, e58387.

Kobayashi, J. and Ishibashi, M. Bioactive metabolites of symbiotic marine microorganisms. *Chemical Reviews,* **1993**, *93*,1753-1769.

Komaki, H., Ichikawa, N., Hosoyama, A., Fujita, N., and Igarashi, Y. Draft genome sequence of marine-derived *Streptomyces* sp. TP-A0873, a producer of a pyrrolizidine alkaloid bohemamine. *Genome Announcements,* **2015**, *3*, e00008-15.

Koressaar, T. and Remm, M. Enhancements and modifications of primer design program. *Bioinformatics*, **2007,** *23*, 1289-1291.

Kumar, S. Jones, M., Koutsovoulos, G., Clarke, M., and Blaxter, M. Blobology: exploring raw genome data for contaminants, symbionts, and parasites using taxon-annotated GC-coverage plots. *Frontiers in Genetics,* **2013**, *4*, 237.

Lee, D.-S., Yoon, C.-S., Jung, Y.-T., Yoon, J.-H., Kim, Y.-C., and Oh, H. Marine-derived secondary metabolite, griseusrazin A, suppresses inflammation through heme oxygenase-1 induction in activated RAW264.7 Macrophages. *Journal of Natural Products,* **2016**, *79*, 1105-1111.

Li, J. W.-H. and Vederas, J. C. Drug discovery and natural products: end of an era or an endless frontier? *Science,* **2009**, *325*, 161-165.

Lin, Z., Torres, J. P., Tianero, M. D., Kwan, J. C., and Schmidt, E. W. Origin of chemical diversity in prochloron-tunicate symbiosis. *Applied and Environmental Microbiology,* **2016**, *82*, 3450-3460.

Long, E. O., Kim, Hun S., Liu, D., Peterson, M. E., and Rajagopalan, S. Controlling NK cell responses: integration of signals for activation and inhibition. *Annual Review of Immunology,* **2013**, *31*, 227-258.

Lopanik, N. B. Chemical defensive symbioses in the marine environment. *Functional Ecology,* **2014**, *28*, 328-340.

Lu, Z., Liu, D., Hornia, A., Devonish, W., Pagano, M., and Foster, D. A. Activation of protein kinase C triggers its ubiquitination and degradation. *Molecular and Cellular Biology,* **1998**, *18*, 839-845.

Manni, L., Zaniolo, G., Cima, F., Burighel, P., and Ballarin, L. *Botryllus schlosseri*: A model ascidian for the study of asexual reproduction. *Developmental Dynamics,* **2007**, *236*, 335-352.

Moran, N. A., McCutcheon, J. P. and Nakabachi, A. Genomics and evolution of heritable bacterial symbionts. *Annual Review of Genetics,* **2008**, *42*, 165-190.

Oancea, E. and Meyer, T. Protein kinase C as a molecular machine for decoding calcium and diacylglycerol signals. *Cell,* **1998**, *95*, 307-318.

Pores-Fernando, A. T. and Zweifach, A. Calcium influx and signaling in cytotoxic T-lymphocyte lytic granule exocytosis. *Immunological Reviews,* **2009**, *231*, 160-173.

Price, M. N., Dehal, P. S., and Arkin, A. P. FastTree: computing large minimum-evolution trees with profiles instead of a distance matrix. *Molecular Biology and Evolution*, **2009**, *26*, 1641-1650.

Price, M. N., Dehal, P. S., and Arkin, A. P. FastTree 2 -- approximately maximum-likelihood trees for large alignments. *PLoS ON,*. **2010**, *5*, e9490.

Riesenfeld, C. S., Murray, A. E. and Baker, B. J. Characterization of the microbial community and polyketide biosynthetic potential in the palmerolide-producing tunicate *Synoicum adareanum*. *Journal of Natural Products,* **2008**, *71*, 1812-1818.

Rinehart, K. L. Antitumor compounds from tunicates. *Medicinal Research Reviews,* **2000**, *20*, 1-27.

Rowley, A. F. and Powell, A. Invertebrate immune systems–specific, quasi-specific, or nonspecific? *The Journal of Immunology,* **2007**, *179*, 7209-7214.

Sakai, R., Rinehart, K. L., Kishore, V., Kundu, B., Faricloth, G., Gloer, J. B., Carney, J. R., Namikoshi, M., Sun, F., Hughes Jr., R. G., Garcia Gravalos, D., Garcia De Quesada, T.,

Wilson, G. R., and Heid, R. M. Structure-activity relationships of the didemnins. *Journal of Medicinal Chemistry,* **1996**, *39*, 2819-2834.

Schmidt, E. W. and Donia, M. S. Cyanobactin ribosomally synthesized peptides - a case of deep metagenome mining. *Methods in Enzymology,* **2009**, *458*, 576-595.

Schmidt, E. W. and Donia, M. S. Life in cellulose houses: symbiotic bacterial biosynthesis of ascidian drugs and drug leads. *Current Opinions in Biotechnology,* **2010**, *21*, 827-833.

Scofield, V. L., Schlumpberger, J. M., West, L. A. and Weissman, I. A. Protochordate allorecognition is controlled by a MHC-like gene system. *Nature,* **1982**, *295*, 499-502.

Shigemori, H., Bae, M. A., Yazawa, K., Sasaki, T., and Kobayashi, J. Alteramide A, a new tetracyclic alkaloid from a bacterium *Alteromonas* sp. associated with the marine sponge *Halichondria okadai*. *Journal of Organic Chemistry,* **1992**, *57*, 4317-4320.

Takashima, M. and Sakai, H. A new toxic substance, teleocidin, produced by *Streptomyces*. *Bull. Agr. Chem. Soc. Japan,* **1960**, *24*, 647-651.

Taketa, D. A. Nydam, M. L., Langenbacher, A. D., Rodriguez, D., Sanders, E., and De Tomaso, A. W. Molecular evolution and in vitro characterization of *Botryllus* histocompatibility factor. *Immunogenetics,* **2015**, *67*, 605-623.

Tapiolas, D. M., Roman, M., Fenical, W., Stout, T. J., and Clardy, J. Octalactins A and B: cytotoxic eight-membered-ring lactones from a marine bacterium, *Streptomyces* sp. *Journal of the American Chemical Society,* **1991**, *113*, 4682-4683.

Torsten, S. Prokka: rapid prokaryotic genome annotation. *Bioinformatics,* **2014**, *30*, 2068-2069.

Untergasser, A., Cutcutache, I., Koressaar, T., Ye, J., Faircloth, B. C., Remm, M., and Rozen, S. G. Primer3—new capabilities and interfaces. *Nucleic Acids Research,* **2012**, *40*, e115.

Vizzini, A., Di Falco, F., Parrinello, D., Sanfratello, M. A, Mazzarella, C., Parrinello, N., and Cammarata, M. *Ciona intestinalis* interleukin 17-like genes expression is upregulated by LPS challenge. *Developmental and Comparative Immunology,* **2015**, *48*, 129-137.

Wang, S., Liu, M., Lewin, N. E., Lorenzo, P. S., Bhattacharrya, D., Qiao, L., Kozikowski, A. P., and Blumberg, P. M. Probing the binding of indolactam-v to protein kinase c through site-directed mutagenesis and computational docking simulations. *Journal of Medicinal Chemistry,* **1999**, *42*, 3436-3446.

Watve, M. G., Tickoo, R., Jog, M. M. and Bhole, B. D. How many antibiotics are produced by the genus *Streptomyces*? *Archives of Microbiology,* **2001**, *176*, 386-390.

Weber, T., Blin, K., Duddela, S., Krug, D., Kim, H. U., Bruccoleri, R., Lee, S. Y., Fischbach, M. A., Muller, R., Wohlleben, W., Breitling, R., Takano, E., and Medema, M. H. antiSMASH 3.0—a comprehensive resource for the genome mining of biosynthetic gene clusters. *Nucleic Acids Research,* **2015**, *43*, e237-243.

Zhang, G., Kazanietz, M. G., Blumberg, P. M. and Hurley, J. H. Crystal structure of the Cys2 activator-binding domain of protein kinase Cδ in complex with phorbol ester. *Cell*, **1995**, *81*, 917-924.

Zhao, Z., deMayo, J. A., West, A. M., Balunas, M. J., and Zweifach, A. Development of an enhanced phenotypic screen of cytotoxic t-lymphocyte lytic granule exocytosis suitable for use with synthetic coumpound and natural product collections. *Journal of Biomolecular Screening,* **2016**, *21*, 556-566.